

1  
2  
3  
4  
5  
6  
7  
8  
9  
10  
11  
12  
13  
14  
15  
16  
17  
18  
19  
20  
21  
22  
23  
24

Untangling differentiation in arc lavas: constraints from  
unusual minor and trace element variations at Salak Volcano,  
Indonesia

Heather K. Handley<sup>a\*</sup>, Jon P. Davidson<sup>a</sup>, Colin G. Macpherson<sup>a</sup>, James A. Stimac<sup>b</sup>

<sup>a</sup>Department of Earth Sciences, Durham University, South Road, Durham, DH1 3LE, UK.

<sup>b</sup>Chevron Geothermal and Power, Sentral Senayan I, 11<sup>th</sup> Floor, Jalan Asia Afrika No. 8,  
Jakarta 10270, Indonesia.

\*Corresponding author. [hhandley@els.mq.edu.au](mailto:hhandley@els.mq.edu.au)

1 **Abstract**

2 Volcanic rocks from Salak Volcano in West Java display intriguing minor and trace  
3 element geochemical variations with silica. TiO<sub>2</sub> and P<sub>2</sub>O<sub>5</sub> contents, Y, HFSE and REE  
4 concentrations are abnormally rich in the central vent group (CVG) lavas (e.g. Y = 32-69  
5 ppm; Yb, 3-6.5 ppm) and display striking positive correlations with SiO<sub>2</sub>. This contrasts with  
6 rocks erupted at side vents (SVG) on the eastern and western flanks of Salak and with rock  
7 suites of most other Javan volcanoes where these elements remain relatively constant with  
8 increasing SiO<sub>2</sub>. Modelling of major and trace element data indicate that low pressure  
9 fractional crystallisation exerts strong control on the composition of CVG lavas. HFSE and  
10 HREE data are inconsistent with magma mixing, and can be explained by incompatible  
11 behaviour during fractionation of plagioclase, clinopyroxene and Fe-Ti oxide ± orthopyroxene  
12 and olivine. The observed variations in K/Rb and Ba/Th ratios and correlation of <sup>87</sup>Sr/<sup>86</sup>Sr  
13 with indices of differentiation necessitate assimilation of a low K/Rb, low Ba/Th, Sr-rich  
14 contaminant with <sup>87</sup>Sr/<sup>86</sup>Sr of ~ 0.7048 during fractional crystallisation. For the eastern flank  
15 SVG, deep fractionation of a phase in which HFSE and HREE are compatible (e.g.  
16 amphibole) is implicated. By extension, this is also suggested to occur beneath the majority of  
17 Javan volcanoes. Radiogenic isotope ratios (Sr-Hf-Nd) of Salak lavas are similar to other  
18 Javan lavas. SVG rocks erupted from the eastern flank vent have significantly more primitive  
19 Hf-Nd isotope ratios than other Salak volcanic rocks and may represent the least  
20 contaminated (by arc crust or subduction input) Salak lavas.

21

22 *Key words:* crustal contamination; fractional crystallisation; geochemistry; HFSE;  
23 petrogenesis; Sunda arc

24

1 **1. Introduction**

2 Understanding how geochemical signatures are imparted to arc rocks is problematic.  
3 Element compositions in arc lavas are dependent not only on the composition of the primary  
4 magma from which they originated, but also on the multitude of differentiation processes  
5 primary magma may suffer en route to the Earth's surface. Therefore elucidating  
6 composition-modifying processes in arc lavas is a prerequisite before the nature, composition  
7 and components of the source can be determined. Among the variety of processes capable of  
8 masking element concentrations of primary magmas, fractional crystallisation, crustal  
9 contamination and magma mixing (e.g. Ewart, 1982; Davidson et al., 1987; Hildreth and  
10 Moorbath, 1988; Tepley et al., 2000) are commonly identified in arc lavas.

11 Separate differentiation trends occur in lavas from within the single volcanic centre at  
12 Salak Volcano in West Java, and so this volcano provides a great opportunity to study the  
13 impact of shallow level processes on the composition of arc lavas. The steeply-sloped,  
14 positive correlations of HFSE (high field strength elements) and HREE (heavy rare earth  
15 elements) with indices of differentiation displayed by rocks erupted from the central vent at  
16 Salak are highly unusual compared to most other Sunda arc volcanic rock suites. This paper  
17 constrains the relative importance of various differentiation processes at Salak, in order to  
18 explain the abnormal HFSE-HREE differentiation trends displayed by the central vent  
19 eruptive products and their genetic relationship to flank vent volcanic rocks. This information  
20 is essential before the characteristics of the source can be investigated and it will aid in  
21 elucidating the nature of crust in West Java, of which relatively little is known. We suggest  
22 that fractionation of an (unseen) HFSE-HREE bearing phase plays an important role in the  
23 chemical evolution of most Javan island arc magmas.

24

25 **2. Tectonic setting**

1       Gunung Salak, 2211m, is a prominent stratovolcano located in the Quaternary volcanic  
2 front of the Sunda arc in West Java. The Sunda arc stretches from the Andaman Islands north  
3 of Sumatra to Flores in the Banda Sea and has developed as a result of the 6-7cm<sup>-1</sup> northward  
4 migration and consequent subduction of the Indo-Australian Plate beneath the Eurasian Plate  
5 (Le Pichon, 1968; DeMets et al., 1990; Tregoning et al., 1994). The tectonic features of the  
6 area have been described in detail by Hamilton (1979). Beneath Java (and Salak) the crust is  
7 ~20 km thick and has a 'quasi-continental' seismic velocity structure, intermediate between  
8 continental and oceanic (Ben-Avraham and Emery, 1973, Curray et al., 1977; Jarrard, 1986).  
9 Further east, seismic data indicate that the crust is ~18 km thick near Bali and 5-10 km  
10 beneath Flores (Curray et al., 1977). The south-eastern boundary of Sundaland (SE Asian  
11 continental part of the Sunda block/Eurasian plate with pre-Tertiary basement) is suggested  
12 by Hamilton (1979) to be located in West Java. However, due to limited knowledge of the  
13 precise structure and composition of the Javan crust, the exact location and nature of this  
14 boundary remain unknown.

15

### 16 **3. Geology of Salak and sampling details**

17       Salak forms the north-eastern part of the Salak-Perbakti-Gagak volcanic massif (Fig. 1),  
18 which consists of Upper Pleistocene to Recent stratovolcanoes, parasitic vents and  
19 phreatomagmatic craters. The Perbakti-Gagak range to the south-west is strongly eroded.  
20 Both areas in the north-east and south-west are sites of extensive hydrothermal activity.  
21 Intermittent volcanism occurred at Salak between ~0.2 to 1.2 my ago (Stimac, 2003). In  
22 historic time, volcanic activity at Salak has been limited to a number of phreatic explosions  
23 occurring at side vents on the flanks of the volcano. The summit area of Salak is characterised  
24 by two large breached craters, one open to the northeast and another to the southwest (Fig. 1),  
25 which are associated with volcanic sector collapse events. The westernmost crater was the

1 source of a large debris-avalanche deposit which extends over 10 km from the summit.  
2 Satellitic cones are mainly found on the south-west flank of Salak and on the northern  
3 foothills on the eastern side of the volcano. A late-stage dome built on the western crater rim  
4 is a result of the most recent activity.

5 The volcanic products of Salak can be divided into two main groups based on eruption  
6 location: those erupted from the central vent (CVG) and those erupted from flank or side  
7 vents (SVG). The CVG, consisting of multiple lava flows and pyroclastic units, dominates the  
8 volcanic deposits at Salak and therefore the majority of samples in this study were collected  
9 from this group (filled circles, Fig. 1). SVG samples S102 and S103 were taken from lava  
10 flows erupted from a side vent on the eastern slope of Salak. S107A and S107B SVG samples  
11 are from the western flank. Sampling of SVG products for geochemical analysis on the  
12 western flank was of limited success due to extensive alteration of lava caused by  
13 hydrothermal activity. Sample S112 is from a lava flow (SL3) thought to originate from the  
14 main vent (CVG) (Zaennudin et al., 1993). However, this sample is geochemically similar to  
15 the SVG samples in major and trace element composition. This unit extends down the western  
16 flank of Salak, therefore it is possible that S112 may have been erupted from one of the  
17 western side vents. As a result of uncertainty in the provenance of this sample it is  
18 distinguished from the other samples in all diagrams. Two pumice samples collected on the  
19 western slope of Salak (S100 and S101) are from extensive airfall deposits related to pre-  
20 Salak activity (Zaennudin, et al., 1993). These deposits are overlain by thinner airfall deposits  
21 from Salak. Limited dating has been carried out on Salak-Perbakti-Gagak volcanic products  
22 (Stimac, 2003). Reliance on geological maps and relative stratigraphy in this study limits a  
23 detailed temporal evaluation of Salak lavas and therefore this is not carried out here.

24

#### 25 **4. Analytical techniques**

1 Mineral analyses were performed on carbon-coated polished slides of selected Salak  
2 volcanic rocks using a Cameca SX 100 at the University of Manchester NERC facility. The  
3 accelerating voltage was 15kV and beam current was 2nA. Detection limits (wt%) for Al, Mg,  
4 K, Ca, Ti are 0.01 or lower, Na, Si, Cr, Ni are around 0.03, while Fe is slightly higher around  
5 0.08. Element precision is dependant on the mineral being analysed, but was typically less  
6 than 1% for Ca, Ti, Si, Al and Mg, between 1-2% for Fe, 2.7% for Ni and around 4% for Na,  
7 K, Mn and Cr.

8 Major element contents of Salak whole-rock samples were determined on fused glass discs  
9 produced by the Fusion method (spectroflux 105) using the Automated Philips PW2404 X-ray  
10 fluorescence spectrometer at the University of Edinburgh. In-house rock standards were used  
11 to calibrate the machine and monitor accuracy and precision during analysis.

12 Trace element concentrations of Salak rock powders were determined on the PerkinElmer  
13 ELAN 6000 quadrupole ICP-MS at Durham University following the analytical procedure  
14 and instrument operating conditions described by Ottley et al. (2003). Multiple analyses of  
15 procedural blanks (3 per batch), in-house standards and international reference materials: W2,  
16 BHVO-1, AGV1, BE-N and BIR1 during each session e.g. at the start, mid-way, and at the  
17 end of a run, allowed any drift in the instrument calibration to be detected. Reproducibility  
18 (internal and external) of standard values on the ELAN were less than 5% relative standard  
19 deviation.

20 Preparation of whole rock powders for Sr, Nd and Hf isotope analysis was undertaken in  
21 the Arthur Holmes Isotope Geology Laboratory (AHIGL) at Durham University. The sample  
22 dissolution procedure and chemical separation of Hf and Nd from rock samples is based on  
23 that presented by Dowall et al. (2003). The separation procedure for Sr follows that detailed  
24 by Charlier et al. (2006) except Sr was collect from the column in 300  $\mu$ L MQ (rather than  
25 0.05M HNO<sub>3</sub>) followed by addition of 15  $\mu$ L 10M HNO<sub>3</sub> to the collected Sr fraction. Sr, Nd

1 and Hf isotope ratios were determined on the AHIGL ThermoElectron Neptune Multi-  
2 collector Plasma Mass Spectrometer (MC-ICP-MS). Details of instrument operating  
3 conditions are presented in Nowell et al. (2003) and Dowall et al. (2003). Instrumental mass  
4 bias was corrected for using a  $^{88}\text{Sr}/^{86}\text{Sr}$  ratio of 8.375209 (the reciprocal of the  $^{86}\text{Sr}/^{88}\text{Sr}$  ratio  
5 of 0.1194),  $^{146}\text{Nd}/^{145}\text{Nd}$  ratio of 2.079143 (equivalent to the more commonly used  $^{146}\text{Nd}/^{144}\text{Nd}$   
6 ratio of 0.7219) and  $^{179}\text{Hf}/^{177}\text{Hf}$  ratio of 0.7325 plus an exponential law. Data quality was  
7 monitored over several analytical sessions by regular analysis of standard reference materials  
8 during each run. The reproducibility of the  $^{87}\text{Sr}/^{86}\text{Sr}$ ,  $^{143}\text{Nd}/^{144}\text{Nd}$  and  $^{176}\text{Hf}/^{177}\text{Hf}$  ratios for the  
9 respective standard solutions in each of the individual analytical sessions are better than 21  
10 ppm in all cases. Sr-Nd-Hf isotope data presented are plotted relative to NBS 987, J&M and  
11 JMC 475 standard values of 0.71024 (Thirlwall, 1991), 0.511110 (Royse et al., 1998) and  
12 0.282160 (Nowell, et al., 1998) respectively. Blank samples processed (at least 2 per sample  
13 batch) were analysed by ICP-MS on the PerkinElmer ELAN 6000 quadrupole at Durham  
14 University. Total analytical blanks for Sr, Nd and Hf were below 1.2 ng for Sr (typically <  
15 300 pg), 219 pg for Nd and 73 pg for Hf. These values are insignificant considering the  
16 quantity of Sr, Nd and Hf processed from the volcanic rocks (12-65  $\mu\text{g}$ , 2-7  $\mu\text{g}$  and 0.5-1.2  $\mu\text{g}$   
17 respectively).

18 Oxygen isotope analyses of mineral separates (~10mg per sample) were determined by  
19 laser-fluorination at Royal Holloway, University of London; using an analytical procedure  
20 following that of Macpherson et al. (2000). In-house standard values of SC olivine 2 and  
21 GMG II during the period of study were within 0.01‰ of accepted values:  $+5.24\text{‰} \pm 0.04$   
22 ( $1\sigma$ ,  $n = 6$ ) and  $+5.69\text{‰} \pm 0.08$  ( $1\sigma$ ,  $n = 15$ ), respectively. Oxygen yields were slightly low,  
23 but consistent over the individual sessions: 93% for plagioclase ( $n = 7$ ) and between 92-94%  
24 ( $n = 20$ ) for clinopyroxene. Replicate analyses of plagioclase and clinopyroxene throughout

1 the study were within 0.09‰ and 0.04‰ respectively. Oxygen results are reported as per  
2 mille deviations relative to the standard mean ocean water (V-SMOW) standard.

3

#### 4 **5. Petrology and mineral chemistry**

5 Modal analyses of Salak lavas and representative mineral compositions are given in Tables  
6 1 and 2-5, respectively. Andesites are the most common rock type sampled at Salak. The  
7 andesites of the SVG are generally more phenocryst rich than those of the CVG with total  
8 phenocryst abundances ranging between ~50-60 % and 20-46 % (modal volume), respectively  
9 (Table 1). Both andesite groups contain a typically observed island-arc mineral assemblage of  
10 plagioclase, clinopyroxene, orthopyroxene and Fe-Ti oxide. Basaltic-andesites of the CVG  
11 contain olivine phenocrysts, which commonly occur with both clinopyroxene and  
12 orthopyroxene (indicating magmatic disequilibrium in the latter case). The olivine  
13 phenocrysts ( $Fo_{54-66}$ , Table 2) are generally small and subhedral, some showing slight  
14 alteration to iddingsite at crystal edges. The SVG rhyolite and Pre-Salak pumice samples are  
15 dominated by glassy groundmass and phenocrysts of plagioclase with minor pyroxene. Small  
16 amounts of amphibole and quartz  $\pm$  biotite are also present (Table 1).

17 Orthopyroxene phenocrysts in the basaltic-andesites of the CVG are mostly subhedral-  
18 euhedral and infrequently contain smaller inclusions of early-formed olivine (S104). In some  
19 basaltic-andesites (S104, S105 and S108) the orthopyroxene phenocrysts are surrounded by a  
20 thin rim, or jacket of clinopyroxene. This disequilibrium feature appears to be relatively  
21 common in arc lavas and has been observed in the volcanic products of several Javan  
22 volcanoes: Ijen (Sitorus, 1990), Slamet (Vukadinovic and Sutawidjaja, 1995), Lamongan  
23 (Carn and Pyle, 2001) and Gede (Handley, 2006). Mineralogically, clinopyroxene and  
24 orthopyroxene in the basaltic andesites of the CVG lack evidence for compositional  
25 disequilibrium, displaying normal zoning of phenocrysts from Mg-rich cores towards more

1 Fe-rich rims. Orthopyroxene and clinopyroxene compositions available for the andesites show  
2 slightly more variation in the SVG than the CVG (Figs. 2a & b). The limited pyroxene  
3 analyses available for the SL3 lava show restricted compositional variation (Fig. 2c).

4 Plagioclase is the most abundant phenocryst phase in all CVG and SVG rocks. Plagioclase  
5 phenocrysts exhibit a wide range in composition in the basaltic-andesites of the CVG (Figs.  
6 3a & b; Table 4), with plagioclase rims displaying the largest variation in anorthite content  
7 ( $An_{58-91}$ ). Phenocryst interiors are more restricted in composition and have fairly high An  
8 contents (above 80). The An contents of several plagioclase rims are higher than those in  
9 respective groundmass plagioclase ( $< An_{55}$ ) indicating that not all phenocrysts were in  
10 equilibrium with the host liquid. Disequilibrium textures of plagioclase phenocrysts  
11 (oscillatory zoning, sieve textures and infrequent resorbed cores) are observed in all CVG  
12 basaltic-andesite samples. CVG and SVG andesites display similar compositional ranges in  
13 plagioclase (Table 4). In the CVG (Fig. 3c) plagioclase phenocryst and groundmass  
14 compositions are extremely homogeneous ( $An_{48-59}$ ) with the exception of one core analysis  
15 ( $An_{72}$ ). The SVG plagioclases display a slightly wider compositional range and often the core  
16 sections possess lower anorthite contents than respective mid and rim sections (Fig. 3e). Sieve  
17 textures and oscillatory zoning are common in plagioclase phenocrysts of both groups of  
18 andesites. The SL3 andesite displays a fairly restricted range in plagioclase composition  
19 ( $An_{54-68}$ ) similar to the andesite analysed from the CVG (Fig. 3d). Some SL3 plagioclase  
20 phenocrysts show reverse zoning from less An-rich cores to more An-rich rims.

21 Fe-Ti oxide (titanomagnetite) occurs as a phenocryst phase in all rocks and is often  
22 associated with the other mafic phases, commonly occurring as inclusions within pyroxene, or  
23 forming a glomerocrystic texture with pyroxene. Titanomagnetite is slightly more Ti-rich in  
24 the CVG andesite compared to the SVG andesite (Table 5).

1 Cognate xenoliths are observed in SVG samples from the eastern flank unit, PD1 (S102  
2 and S103), displaying sharp contacts with the surrounding lava. The xenoliths are composed  
3 of heavily sieve-textured and oscillatory-zoned plagioclase phenocrysts, clinopyroxene,  
4 orthopyroxene and Fe-Ti oxide phenocrysts (titanomagnetite and ilmenite; in close  
5 association with ferromagnesian minerals) set in a medium-grained groundmass. The  
6 groundmass is dominated by euhedral plagioclase laths, elongate acicular pyroxene, small  
7 oxide crystals and minor devitrified glass. Clinopyroxene occasionally forms thick jackets  
8 around orthopyroxene phenocrysts. Fig. 2b shows there is some overlap in clinopyroxene and  
9 orthopyroxene compositions between the xenolith (black crosses) and the host rock (open  
10 squares). However, orthopyroxene phenocrysts in the xenolith also contain significantly more  
11 En-rich compositions. Plagioclase compositions in the xenolith (Fig. 3f) are scattered, but  
12 generally more An-rich than those in the host lava (Fig. 3e).

13

## 14 **6. Geochemistry**

### 15 *6.1. Major and trace element variations*

16 Major and trace element data are reported in Table 6. Salak lavas are relatively evolved,  
17 with MgO contents less than 4 wt %. Salak volcanic rocks display negative correlations on  
18 diagrams of Al<sub>2</sub>O<sub>3</sub>, Fe<sub>2</sub>O<sub>3</sub>, MgO and CaO against SiO<sub>2</sub>, and positive correlations between  
19 SiO<sub>2</sub> and both K<sub>2</sub>O and Na<sub>2</sub>O (Fig. 4), although Na<sub>2</sub>O contents in the SVG are relatively  
20 constant with increasing SiO<sub>2</sub>. TiO<sub>2</sub> and P<sub>2</sub>O<sub>5</sub> variation is split into two markedly different  
21 trends. Lavas erupted from the CVG generally show an increase in TiO<sub>2</sub> and P<sub>2</sub>O<sub>5</sub> contents  
22 with increasing SiO<sub>2</sub>, whereas SVG lavas possess lower TiO<sub>2</sub> and P<sub>2</sub>O<sub>5</sub> contents and plot  
23 within the field of other Javan volcanic rocks (Figs. 4g and h). TiO<sub>2</sub> and P<sub>2</sub>O<sub>5</sub> contents  
24 measured in the more evolved CVG rocks (~60% SiO<sub>2</sub>) are unusually high (up to 1.18 and  
25 0.48 wt%, respectively) when compared to the majority of values reported for other Javan

1 lavas (Fig. 4g) and from volcanic rocks of other island arc systems at comparable silica  
2 content e.g. Kermadec (Gamble et al., 1993; Ewart et al., 1994; Turner et al., 1997), Lesser  
3 Antilles (Thirlwall et al., 1996; Zellmer et al., 2003) and Mariana (Woodhead, 1989; Elliot et  
4 al., 1997). Increasing  $\text{TiO}_2$  content with increasing silica (Fig. 4g) is not normally observed in  
5 arc andesites, most probably due to the early fractionation of magnetite (Gill, 1981; Pearce,  
6 1982).

7 The high field strength elements (HFSE) and the rare earth elements (REE), particularly  
8 the heavy REE, also show abnormally high concentrations in the more evolved CVG samples  
9 (Y = 32-69 ppm; Yb, 3-6.5 ppm) and display strikingly positively-sloped, linear trends on  
10  $\text{SiO}_2$  variation diagrams (Figs. 5a and b). This contrasts again with the SVG rocks and the  
11 majority of other volcanic rock suites of Java, where concentrations remain relatively constant  
12 with increasing  $\text{SiO}_2$  (Figs. 5a and b). High concentrations of  $\text{TiO}_2$ ,  $\text{P}_2\text{O}_5$ , Y and systematic  
13 increases of these elements with  $\text{SiO}_2$  are so far only evident at one other volcano in Java,  
14 namely Tengger Caldera in East Java (Figs. 4g and h and 5a). This unusual feature was not  
15 noted in the study of Tengger Caldera by van Gerven and Pichler (1995). Extensive  
16 comparisons of trace element variations between Tengger Caldera and Salak are however  
17 restricted due to the limited geochemical data available for the former volcanic system. In  
18 contrast to the separate HFSE and REE variation trends displayed by the CVG and SVG,  
19 variations in large ion lithophile elements (LILE) are similar, displaying positive correlations  
20 with  $\text{SiO}_2$  (Figs. 5e and f). Sr generally decreases as  $\text{SiO}_2$  increases within each group (Fig.  
21 5g). The SVG rocks containing around 60 wt%  $\text{SiO}_2$  are slightly displaced below the main  
22 Salak trend in the majority of these diagrams with the exception of Sr, where they sit at  
23 slightly elevated values.

24 Chondrite normalised REE patterns of selected Salak lavas are displayed in Fig. 6. Salak  
25 volcanic rocks are enriched in the light REE compared to mid-ocean ridge basalts (Normal-

1 MORB and Indian Ocean-MORB). With the exception of the high silica rhyolite, the heavier  
2 REE show concentrations more similar to those in MORB than the light REE. The higher  
3 silica CVG andesite is located parallel to, but at higher REE concentrations than the less  
4 evolved CVG rock. The enrichment of the REE in the evolved CVG sample is made clear  
5 when compared to a SVG rock of comparable silica content (unfilled squares). Strong  
6 depletions are observed in the middle to heavy REE concentrations of the high SiO<sub>2</sub> (west  
7 flank) SVG rocks, compared to less evolved Salak rocks.

8

## 9 *6.2. Radiogenic isotopes*

10 Sr, Nd and Hf isotope data are presented in Table 6 and shown in Figs. 7 and 8. <sup>87</sup>Sr/<sup>86</sup>Sr  
11 and <sup>143</sup>Nd/<sup>144</sup>Nd isotope ratios of Salak volcanic rocks define a negative array, lying within  
12 the field of previously published Java data. Salak exhibits a relatively wide range in <sup>87</sup>Sr/<sup>86</sup>Sr  
13 ratios, 0.704262 to 0.705051, although the majority of the lavas are more tightly constrained  
14 within the range 0.704569-0.705051. The two SVG samples, S102 and S103, erupted on the  
15 eastern flank of Salak are displaced from the rest of the Salak lavas, possessing significantly  
16 lower <sup>87</sup>Sr/<sup>86</sup>Sr and higher <sup>143</sup>Nd/<sup>144</sup>Nd ratios (Fig. 7 inset). In Hf-Nd isotope space (Fig. 8),  
17 Salak volcanic rocks also lie within the field defined by Java, possessing lower <sup>143</sup>Nd/<sup>144</sup>Nd  
18 and <sup>176</sup>Hf/<sup>177</sup>Hf isotope ratios than MORB, and higher ratios than Indian Ocean sediments.  
19 The eastern-flank SVG samples, S102 and S103, possess significantly more primitive  
20 <sup>176</sup>Hf/<sup>177</sup>Hf isotope ratios compared to the other Salak lavas (Fig. 8 inset).

21

## 22 *6.3. Stable isotope data*

23 Oxygen isotope data from mineral separates are presented in Table 7. The restricted  
24 clinopyroxene and plagioclase analyses of Salak lavas have low δ<sup>18</sup>O values ranging from  
25 +5.18 to +5.44‰ (n = 3) and +5.96 to +6.07‰ (n = 4), respectively. The former values are

1 similar to mantle clinopyroxene  $\delta^{18}\text{O}$  values reported by Matthey et al. (1994) and Ionov et al.  
2 (1994):  $+5.57 \pm 0.32\text{‰}$  and similar to or slightly lower than those reported from other  
3 volcanoes in Java (Galunggung, Harmon and Gerbe, 1992; Gede Volcanic Complex,  
4 Handley, 2006; Ijen Volcanic Complex, Handley et al., 2007). Plagioclase  $\delta^{18}\text{O}$  values of  
5 Salak are generally higher than those of Galunggung ( $+5.6$  to  $+6.0\text{‰}$ , Harmon and Gerbe,  
6 1992), but lower than those analysed in Merapi volcanics ( $+6.5$  to  $+7.00\text{‰}$ , Gertisser and  
7 Keller, 2003a). Differences in  $\delta^{18}\text{O}$  values between coexisting plagioclase and clinopyroxene  
8 ( $\Delta_{\text{plag-cpx}}$ ) are between  $0.63$  to  $0.79\text{‰}$  and suggest most of the mineral pairs record oxygen  
9 isotopic equilibrium at typical magmatic temperatures for andesite liquids. The limited  
10 number of analyses from Salak prohibits intra-group comparisons of  $\delta^{18}\text{O}$  data, however, the  
11 lowest  $\delta^{18}\text{O}$  clinopyroxene value is measured in the sample with the most primitive radiogenic  
12 isotope ratios (SVG, S103).

13

## 14 **7. Discussion**

15 Minor and trace element variations at Salak are intriguing, and raise two important  
16 questions: 1) Why do the CVG display atypical differentiation trends and unusually high  
17 concentrations in minor and trace elements, in particular for the HREE, Y,  $\text{TiO}_2$  and  $\text{P}_2\text{O}_5$   
18 compared to other Javan volcanoes? 2) Why are there strikingly different differentiation  
19 trends in lavas from a single volcanic centre?

20 Assuming that variations in the silica content of volcanic rocks are generated as a result of  
21 differentiation of magma (Gill, 1981; Davidson et al., 2005), systematic increases of Y, Yb,  
22  $\text{TiO}_2$  and  $\text{P}_2\text{O}_5$  with  $\text{SiO}_2$  within the CVG (Figs. 5a & b and Figs. 4g & h, respectively) are  
23 compelling evidence for geochemical variation being imparted during differentiation in the  
24 crust e.g. through magma mixing, fractional crystallisation and/or combined assimilation and  
25 fractional crystallisation.

1

## 2 *7.1. Differentiation in the Central Vent Group*

### 3 *7.1.1. Magma Mixing*

4 Magma mixing is identified as an important composition-modifying process within the  
5 evolution of many arc magmas (e.g. Conrad et al., 1983; Tepley et al., 2000) including some  
6 Sunda arc magmas (Slamet, Reubi et al., 2002; Merapi, Gertisser and Keller, 2003b; Batur,  
7 Reubi and Nicholls, 2004). Linear correlations displayed by the CVG rocks on bivariate  
8 element-silica diagrams (Figs. 4 and 5) suggest that chemical variation within this group may  
9 be explained by the interaction and mixing of chemically distinct magmas. Phenocryst  
10 textures and mineral disequilibria in CVG lavas (section 5) indicate that open system  
11 processes may have occurred at one or several points in the magmatic evolution of the CVG.

12 A purely geochemical approach to evaluate mixing processes utilises element ratios  
13 (Langmuir et al., 1978; Vogel, 1982; Flood et al., 1989). Magma mixing should produce  
14 hyperbolic arrays in plots of a trace element ratio versus a concentration. Figs. 9a and b show  
15 that the CVG data largely define a curved array on some element-ratio diagrams. K/Rb and  
16 Ba/Th ratios were chosen as these ratios correlate with SiO<sub>2</sub> and display a wide range in the  
17 CVG. The former ratio is also a potentially useful monitor of crust-magma interaction  
18 (Davidson, 1987, Hildreth & Moorbath, 1988), providing that the melt and crust have  
19 distinctive values for the ratio. K/Rb and Ba/Th ratios are plotted against Rb (which  
20 represents the degree of magmatic differentiation) and Yb (to check whether the model can  
21 account for the highly unusual variations in concentrations observed for this element). The  
22 results of bulk-mixing calculations between one of the least evolved CVG samples (S106B)  
23 and several end members are shown in Figs. 9a and b. If element variation in the CVG is a  
24 result of simple mixing, the other end member must be more evolved (higher SiO<sub>2</sub>) in  
25 composition. Granite xenoliths found within a deposit of cream tuff in the Perbakti-Gagak

1 area adjacent to Salak provide evidence for the presence of evolved, granitic material (Stimac,  
2 2003) in West Java. No data are available from this granite for use in modelling, therefore the  
3 more evolved end member magmas in mixing calculations are represented by a rhyolite from  
4 Salak (S107A) and by arc-related granites from some of the southern-most plutonics in  
5 Sumatra (i.e. close to West Java): monzodiorite (75413) and granodiorite (75415) (Gasparon,  
6 1993). Mixing with a more basic end member (tholeiitic lava) from Guntur in West Java  
7 (Edwards, 1990) is also shown for comparison. The end member compositions used in mixing  
8 calculations are given in Table 8.

9 Fig. 9a shows that mixing in K/Rb-Rb space between S106B and a granitic sample with a  
10 high K/Rb ratio (MM D) is unable to generate a mixing curve to fit the CVG data. Similar  
11 unsatisfactory mixing trends would result from mixing with bulk upper-crustal material,  
12 which also has relatively high K/Rb (~250; Taylor, 1977). Mixing between S106B and  
13 granodiorite (MM B) or Javan tholeiite (MM C) also fail to fit the data, generating curves that  
14 have a large decrease and increase (respectively) in K/Rb ratio, with only a small change in  
15 Rb. The mixing curve produced using the Salak rhyolite (MM A) as the evolved end member,  
16 produces the best fit to the CVG data. Fig. 9b, Ba/Th-Yb, shows mixing curves generated  
17 between the same end members in Fig. 9a. Mixing in all cases is inadequate in explaining the  
18 Salak CVG data due to the low Yb content of the end members chosen. Low Yb contents of  
19 basic and evolved Javan lavas and evolved Sumatran plutonics, suggests that Yb contents of  
20 the CVG cannot be explained by simple mixing.

21

### 22 *7.1.2. Fractional crystallisation*

23 Fractional crystallisation was modelled by least squares analysis of Salak major element  
24 data using the XLFRAC programme (Stormer and Nicholls, 1978; Table 9). The results  
25 suggest that the most evolved CVG lava can be produced by fractionation of the least evolved

1 CVG lava by 61% crystallisation ( $\Sigma r^2 = 0.13$ ; model 1). Smaller values of  $\Sigma r^2$  are obtained in  
2 models to less differentiated final lavas (models 2 & 3), regardless of whether orthopyroxene  
3 or olivine is included in the mineral assemblage (compare models 3 & 4). This suggests that  
4 major and minor element variation within the CVG can be explained by fractional  
5 crystallisation of plagioclase, clinopyroxene, Fe-Ti oxide +/- olivine and orthopyroxene (e.g.  
6 Figs. 4g and h). But, can fractional crystallisation explain the unusual trace element variation  
7 trends not seen in the majority of Javan lavas using the same mineral assemblage?

8 Y and the REE often behave as incompatible elements in primitive arc tholeiites, however  
9 they usually remain constant or decrease in concentration with increasing magmatic  
10 fractionation in the calc-alkaline series, where they can be accommodated within amphibole,  
11 apatite and zircon (Pearce, 1982). This is exemplified by the Java data in Figs. 4g and h, and  
12 amphibole fractionation curves in Figs. 5a and b. To examine whether fractional  
13 crystallisation can produce the large increases in Y, Yb and Ti of the CVG (over a relatively  
14 narrow range in silica) and test the conclusions of least squares analysis, simple calculations  
15 were made using the Rayleigh fractionation equation:  $C_l = C_o F^{(D-1)}$  where  $C_l$  is the  
16 concentration of an element in the liquid,  $C_o$  is the concentration of an element in the original  
17 liquid,  $F$  is the fraction of liquid remaining and  $D$  is the bulk distribution coefficient. The  
18 degree of fractionation ( $F$ ) and the phase proportions used are those suggested by major  
19 element modelling (Table 9, model 1). The distribution coefficients used are given in Table  
20 10. Calculated Ti, Y and Yb compositions expected in the daughter rocks (Table 10, Figs. 4g,  
21 5a and b) show that incompatible behaviour of HFSE and HREE during fractional  
22 crystallisation can account for the high concentrations of these elements in Salak rocks. In all  
23 three models in Table 10 the concentrations predicted in the daughter rocks are higher than  
24 those actually measured. This contrasts with the results of mixing (Fig. 9b) between a basic  
25 CVG rock and the tholeiitic and more evolved volcanic and plutonic samples, which were

1 unsuccessful in accounting for high Yb concentrations. Fractional crystallisation curves (FC)  
2 are shown on K/Rb-Rb and Ba/Th-Yb diagrams (Figs. 9a and b) for removal of the same  
3 mineral assemblage used above. It should be noted that an identical FC curve is produced if  
4 the modal mineral assemblage of S106B (Table 1) is used instead. The Salak CVG data  
5 diverge from the calculated FC curve towards lower K/Rb and Ba/Th, thus suggesting that  
6 pure closed-system fractional crystallisation cannot explain all of the geochemical variation  
7 observed in the CVG lavas.

8

### 9 *7.1.3. Assimilation and Fractional Crystallisation (AFC)*

10 AFC processes are recognised in the evolution of magma in arc settings (Davidson et al.,  
11 1987; Hildreth and Moorbath, 1988; Davidson and Harmon, 1989) and have been suggested  
12 for the Sunda arc (Gasparon et al., 1994). Little is known about the nature and composition of  
13 the crust in West Java. Seismic velocities suggest that the crust in West Java is thicker than  
14 that at the eastern end of Java (Ben-Avraham and Emery, 1973; Curray et al., 1977;  
15 Kieckhefer et al., 1980) and in West Java the arc may be built on continental material, i.e.  
16 Sundaland pre-Tertiary basement (Hamilton, 1979). Large granite blocks found in a tuff  
17 deposit in the vicinity of Salak (Perbakti-Gagak area, Fig. 1) display partially melted margins  
18 with adhering rhyolitic lava (Stimac, 2003). It is unknown when this granite was emplaced in  
19 the crust, but it suggests that interaction and possible contamination of magma by evolved  
20 plutonic rocks may occur at Salak. AFC curves are shown on Figs. 9a and b for contamination  
21 of the most basic Salak magma, by evolved volcanic (AFC A) and plutonic (AFC B) rocks,  
22 possessing low K/Rb and Ba/Th ratios. These curves fit the array of Salak data well, even  
23 though the contaminants possess low Yb concentrations (cf. mixing) Assimilation of upper  
24 and bulk crust (e.g. Taylor, 1977; Sumatran granitoid 75413) would generate concave-down  
25 AFC curves, inconsistent with the CVG data. It was suggested by Hamilton (1979) that the

1 crust in West Java is not truly silicic in character and may consist of older volcanic-arc rocks  
2 and ophiolite slivers. However, AFC models involving basic arc rocks (e.g. Fig. 9 AFC C)  
3 and a range of basic and ophiolite compositions (see below) are also inconsistent with the  
4 CVG array.

5 In summary, major and trace element modelling suggests that the unusual increases in  
6 HFSE and HREE with increasing SiO<sub>2</sub> are created due to incompatible behaviour of these  
7 elements during fractional crystallisation. Systematic variations in some trace element ratios  
8 (K/Rb and Ba/Th) and disequilibrium textures observed in the rocks indicate that assimilation  
9 of a contaminant with low K/Rb and Ba/Th ratios occurs during fractional crystallisation in  
10 the crust.

11

#### 12 ***7.1.4. Isotopic constraints***

13 Continental-type crustal rocks commonly have elevated <sup>87</sup>Sr/<sup>86</sup>Sr isotope ratios compared  
14 to Quaternary volcanic rocks and mantle-derived magmas. Assimilation of crust during  
15 crystal fractionation (DePaolo, 1981) in arc magmas may therefore cause modification to the  
16 isotope ratios in resultant lavas. Consequently, a plot of Sr isotope ratio against an index of  
17 differentiation, e.g. SiO<sub>2</sub>, can be used to detect AFC processes, in cases where the crust being  
18 assimilated is isotopically distinct. Even though the number of samples with isotope data is  
19 relatively limited and the variation in <sup>87</sup>Sr/<sup>86</sup>Sr of the CVG is small, the more evolved CVG  
20 samples display generally higher <sup>87</sup>Sr/<sup>86</sup>Sr ratios (Fig. 10), and the data patterns observed in  
21 this plot are identical (though the inverse) to those of Ba/Th with SiO<sub>2</sub> (see inset to Fig. 10).  
22 This suggests that Ba/Th, for which there is more data compared to <sup>87</sup>Sr/<sup>86</sup>Sr, might serve as a  
23 proxy for isotopic composition. The roughly hyperbolic trend observed in Fig. 10 and  
24 variation in <sup>87</sup>Sr/<sup>86</sup>Sr isotope ratio with SiO<sub>2</sub> in the CVG further support control by  
25 differentiation, and more specifically by AFC processes.

1 The five CVG data points define a concave-down hyperbola on Ba/Th versus  $^{87}\text{Sr}/^{86}\text{Sr}$  (Fig.  
2 11). The AFC curves displayed here are for the same AFC end members used in trace element  
3 modelling (see Fig. 9 caption for details). Neither model on Fig. 11 using evolved volcanic  
4 nor plutonic rocks produces hyperbolic curves to fit the CVG data. AFC curves for these  
5 models largely follow the same vertical trend shown by fractionation crystallisation (FC)  
6 alone (arrow, Fig. 11), and altering the rate ratio of mass assimilated to mass crystallised ( $r$ )  
7 has little effect on the shape of the curve. The basic contaminant (see captions to Figs. 9 and  
8 10 for details) produces an AFC curve (C) with a much better fit to the CVG data, but  
9 suggests a large amount of contamination is required compared to crystallisation ( $r = 0.8$ ).  
10 Such high AFC  $r$ -values are not unreasonable and have been proposed for differentiation of  
11 basalts at Jebel Marra volcano in Sudan (Davidson and Wilson, 1989) and by Bourdon et al.  
12 (1998) for the Grande Comore volcanics.

13 A contaminant with a significantly higher Sr content than that of the parental rock would  
14 be able to generate a hyperbola curving in the required direction from the parental  
15 composition of S106B and not necessitate such a high  $r$ -value. Fig. 10 also indicates this as  
16 assimilation of a contaminant with low Sr concentration would produce a concave-up curve  
17 initially projecting in a horizontal direction away from the least evolved CVG sample, which  
18 is inconsistent with the concave-down data array in Fig. 10. The apparent plateau in  $^{87}\text{Sr}/^{86}\text{Sr}$   
19 isotope ratio in  $\text{SiO}_2$ -rich CVG rocks suggests that the  $^{87}\text{Sr}/^{86}\text{Sr}$  ratio of the contaminant is  
20 asymptotic to the  $^{87}\text{Sr}/^{86}\text{Sr}$  ratio of the more evolved CVG samples (i.e.  $\sim 0.7048$ ). If the  
21 distribution coefficient for Sr in plagioclase is greater than one, then a magma crystallising  
22 this phase would become progressively more sensitive to Sr in the contaminant (which is  
23 assumed to be fixed). The more AFC magma endures, the more isotopically sensitive to the  
24 contaminant it would become, and therefore, for a given shift in silica the magma would  
25 obtain a larger shift in  $^{87}\text{Sr}/^{86}\text{Sr}$  isotope ratio if the contaminant had a higher  $^{87}\text{Sr}/^{86}\text{Sr}$  ratio.

1 Consequently, it is argued that if the data are consistent with AFC, the contaminant has a high  
2 Sr concentration and Sr-isotope ratio  $\sim 0.7048$  (curved arrow, Fig. 10) contamination by a high  
3  $^{87}\text{Sr}/^{86}\text{Sr}$  component would result in a data array with a steeper positive correlation on Fig. 10  
4 (diagonal arrow). The moderate decrease in Sr concentration with increasing  $\text{SiO}_2$  in the CVG  
5 (despite the modelled involvement of large amounts of plagioclase fractionation) further  
6 argues for a high-Sr assimilant. An AFC calculation using S106B as the parent magma and  
7 the Sumatran granodiorite as the contaminant suggest that to produce a concave-down  
8 hyperbola to fit the data in Fig. 11 an extremely unrealistic Sr concentration in the  
9 contaminant of  $>7000$  ppm is required. Evolved volcanic or plutonic contaminant end  
10 members are unlikely to possess higher Sr concentrations than the basaltic andesite S106B  
11 being contaminated as Sr content generally decreases with differentiation in arc-related  
12 igneous rocks due to plagioclase fractionation. Incorporation of the assimilant as a partial melt  
13 (0.1 - 10% melting), rather than bulk addition of this component, does not increase the Sr  
14 concentration sufficiently enough to improve the fit of the models for Ba/Th versus Sr isotope  
15 ratio and also leads to a more rapid decrease in Ba/Th ratio, creating an AFC trend further  
16 away from the CVG array.

17 If Sr isotope variation in the CVG is controlled by AFC processes as suggested above, then  
18 the contaminant is characterised by high Sr concentration,  $^{87}\text{Sr}/^{86}\text{Sr}$  isotope ratio of around  
19 0.7048 and low K/Rb and Ba/Th ratios ( $< \sim 110$  and  $< \sim 45$ , respectively). Table 11 shows  
20 trace element data and Sr-isotope ratios for a variety of rocks that may represent the West  
21 Javan crust and could therefore be potential contaminants. However, none of the samples  
22 listed possess all of the required criteria envisaged for the contaminant, therefore at present, a  
23 suitable contaminant is unidentified.

24

## 1 7.2. Relationship of the SVG to the CVG

2 If increases in HFSE and HREE with increasing silica in CVG rocks can be explained by  
3 highly incompatible behaviour during differentiation, then relatively low and decreasing  
4 HFSE and HREE concentrations in the SVG lavas may indicate relatively more compatible  
5 behaviour of these elements during differentiation of SVG magmas. A distinct difference in  
6 the type or abundance of phases crystallising from the magma may therefore be expected.  
7 However, there is little difference between the mineralogies of the CVG and the eastern flank  
8 SVG volcanic rocks. In contrast, the western flank SVG samples have small amounts of  
9 amphibole (hornblende) in their modal mineralogies (Table 1). Strong depletions in HREE  
10 and the steep decrease from La-Sm shown by the western flank SVG samples, relative to  
11 those with lower silica content from the eastern flank (Fig. 6), suggests that very late-stage  
12 fractionation of hornblende ( $\pm$  accessory phases) may account for the relatively low HREE  
13 and HFSE concentrations in these highly evolved samples (cf. deep, early-stage  
14 fractionation). The similarly shaped REE profiles and modal mineralogies of the CVG and  
15 SVG lavas with  $<70$  wt %  $\text{SiO}_2$  precludes a similar explanation for the differences observed  
16 in the geochemistry of these samples.

17 In addition to mineralogical differences, isotopic differences also occur between the  
18 western and eastern flank SVG lavas (Figs. 7 and 8 insets). The western vent SVG rocks are  
19 isotopically similar to the CVG group and may, therefore, be genetically related to each other,  
20 sharing a similar source and evolutionary history. The notably more primitive radiogenic  
21 isotope ratios of the eastern flank SVG lavas suggest that they may have evolved from an  
22 isotopically distinct source, or may represent the least contaminated (either by arc crust or a  
23 subduction component) Salak lava. In the latter case, they reveal the best estimate of least  
24 modified mantle wedge isotopic composition beneath Salak. The similar REE patterns of the  
25 lower  $\text{SiO}_2$  SVG and lower  $\text{SiO}_2$  CVG lavas (Fig. 6), suggests the magmatic source region of

1 the two groups probably contained a comparable mineralogy and underwent similar degrees  
2 of melting.

3 Trace element ratios of HFSE and HREE (e.g. Zr/Nb, Y/Nb) are often used to investigate  
4 the source characteristics of magmas (McCulloch and Gamble, 1991; Woodhead et al., 1993;  
5 Reubi and Nichols, 2004). However, the limited number of samples from the SVG, combined  
6 with the relatively differentiated nature of all Salak lavas and the uncertainty of HFSE/HREE  
7 concentrations in less differentiated samples (due to unusual increases of these elements in the  
8 CVG) hampers this approach at Salak

9 A schematic diagram showing the proposed evolution of magma beneath Salak is displayed  
10 in Fig. 12. Petrographic and radiogenic isotope data suggest that the high SiO<sub>2</sub> SVG rocks  
11 from the western flank vent may be related to the CVG lavas, evolving to lower HFSE and  
12 REE concentrations due to prolonged residence in the crust and the late-stage fractionation of  
13 hornblende ( $\pm$  accessory phases) prior to eruption (A). However, the lower SiO<sub>2</sub> (and  
14 isotopically more primitive) eastern SVG lavas are proposed to have taken a separate  
15 evolutionary pathway to the surface. Low concentrations of HFSE and HREE in these  
16 samples may be the result of fractionation of a HFSE-REE-compatible phase at depth (B),  
17 such as amphibole, which effectively inhibits the relative increase of these elements during  
18 fractional crystallisation at shallower levels. A number of factors control amphibole  
19 fractionation from magma (see Davidson et al. 2007 for a recent discussion), which include  
20 the water content of the magma and also the pressure of crystallisation. Therefore, an apparent  
21 lack of deep-seated amphibole crystallisation in the CVG may imply that the water content  
22 was not as great in the parental magma, or CVG magmas were not stored at deeper levels in  
23 the arc crust. Other arc studies that support a proposal of multiple independent conduits and  
24 reservoirs in the crust beneath active volcanoes include those of Reubi and Nicholls (2004)  
25 and Grove et al. (2005).

1 Within andesitic volcanic rock suites REE concentrations commonly increase with silica  
2 (Gill, 1981). Therefore, due to the relatively constant within suite REE concentrations (black  
3 crosses, Figs. 5b and h) and general lack of hornblende phenocrysts in Javan volcanic rocks,  
4 we speculate that amphibole, or other HFSE-HREE bearing phase, may fractionate at depth  
5 below most Javan volcanoes. Although amphibole-bearing xenoliths have not been found in  
6 Salak lavas, gabbroic xenoliths with variable amphibole contents are observed in lavas  
7 erupted at Sangeang Api volcano in the East Sunda arc (Turner et al., 2003) and gabbroic  
8 mafic inclusions composed of plagioclase and amphibole are present in lavas at Merapi  
9 volcano in Central Java (Camus et al., 2000).

10

## 11 **8. Conclusions**

12 Unusual HFSE and HREE variation trends (compared to most other volcanic rocks from  
13 Java) displayed by the CVG lavas of Salak are produced during differentiation in the crust.  
14 Differentiation processes have been modelled to show that: 1) CVG element variation is not  
15 consistent with simple mixing due to the low HFSE and HREE concentrations found in  
16 continental and oceanic crustal end members. 2) Evolution to high HFSE and HREE  
17 concentrations in the CVG can be explained by incompatible behaviour of these elements  
18 during fractional crystallisation. 3) Variation in some trace element ratios (K/Rb and Ba/Th)  
19 of the CVG suggest assimilation of crust also occurs during fractional crystallisation of the  
20 magma. AFC modelling and  $\delta^{18}\text{O}$  data suggest that typical continental-type upper-crustal  
21 contaminants are not likely to be involved in AFC processes at Salak (cf. the Andes and  
22 Lesser Antilles, Davidson et al., 2005 and references therein). Geochemical constraints  
23 suggest that the contaminant is largely similar in geochemical and isotopic composition to the  
24 lavas themselves (e.g. volcanic and/or plutonic arc-related or ophiolitic rocks) and

1 characterised by  $^{87}\text{Sr}/^{86}\text{Sr} \sim 0.7048$ , extremely high Sr concentration and relatively low K/Rb  
2 and Ba/Th ratios.

3 Evolution to high HFSE and HREE concentrations in the CVG lavas suggests that magma  
4 beneath the central part of the volcano has bypassed deep-level storage in the lower crust,  
5 which is envisaged beneath the eastern flank vent. Volcanic rocks of the western flank SVG  
6 display lower HFSE and HREE contents compared to the CVG, which may be explained by  
7 relatively shallow, late-stage hornblende ( $\pm$  accessory phase) fractionation from a CVG-type  
8 parent.

9 HFSE and HREE variations in Salak lavas have drawn attention to the fact that Javan lavas  
10 do not show highly incompatible behaviour of these elements during differentiation. Y and  
11 Yb concentrations in eruptives from the volcanic front on Java display near-horizontal trends  
12 when plotted against silica. With little direct evidence of amphibole fractionation in these  
13 lavas, it is speculated that fractionation of a HFSE-HREE-compatible phase may occur at  
14 depth beneath the majority of volcanoes on Java. Tengger Caldera, in East Java also displays  
15 abnormally steep, Y,  $\text{P}_2\text{O}_5$  and  $\text{TiO}_2$  differentiation trends (similar to the CVG at Salak),  
16 suggesting deep-fractionation of a HFSE-HREE-compatible phase does not take place at this  
17 volcano and further corroborates the idea that the cause is related to crustal-level processes,  
18 rather than isolated source contributions at single volcanic centres in both East and West Java.  
19 This interpretation would benefit greatly from further sampling and geochemical analysis of  
20 Salak SVG deposits, to better constrain differentiation trends within this group and refine the  
21 geochemical models.

22 Finally, the presence of a wide HFSE and HREE variation within a single volcanic centre,  
23 such as that at Salak, emphasises the importance of detailed geochemical study of individual  
24 volcanoes. Arc lavas are generally characterised by high LREE/HFSE ratios, attributed to  
25 involvement of a subducted component. However, LREE/HFSE ratios in Salak lavas are

1 relatively low in the CVG, even though LREE concentrations are relatively high, due to high  
2 HSFE concentrations and positive correlations of both LREE and HFSE with SiO<sub>2</sub> in the  
3 CVG rocks.

4

## 5 **Acknowledgements**

6 We would like to thank Akhmad Zaennudin and colleagues at the Volcanic Survey of  
7 Indonesia in Bandung for invaluable logistical help and guidance in the field. For technical  
8 support and analytical assistance our thanks go to: Geoff Nowell, Chris Ottley and Dave Sales  
9 at Durham University; Dave Plant at the University of Manchester; Dave Lowry at Royal  
10 Holloway University of London; Godfrey Fitton and Dodie James at the University of  
11 Edinburgh. The manuscript was greatly improved by the detailed comments of Bernard  
12 Bourdon and two anonymous reviewers. This project was funded by a NERC studentship  
13 (NER/S/A/2001/06127) and supported by the SEARG at Royal Holloway, University of  
14 London.

15

## 16 **References**

- 17 Alves, S., Schiano, P., Allegre, C.J., 1999. Rhenium-osmium isotopic investigation of Java  
18 subduction zone lavas. *Earth Planet. Sci. Lett.* 168, 65-67.
- 19 Ben-Avraham, Z., Emery, K.O., 1973. Structural framework of Sunda Shelf. *Bull. Amer.*  
20 *Assoc. Pet. Geol.* 57, 2323-2366.
- 21 Ben Othman, D.B., White, W.M., Patchett, J., 1989. The geochemistry of marine sediments,  
22 island arc magma genesis, and crust-mantle recycling. *Earth Planet. Sci. Lett.* 94, 1-21.
- 23 Bottazzi, P., Tiepolo, M., Vanucci, R., Zanetti, A., Brumm, R., Foley, S.F., Oberti, R., 1999.  
24 Distinct site preferences for heavy and light REE in amphibole and the prediction of  
25 Amph/LDREE. *Contrib. Mineral. Petrol.* 137, 36-45.

1 Bourdon, B., Joron, J-L, Claude-Ivanaj, C., Allègre, C.J., 1998. U-Th-Pa-Ra systematics for  
2 the Grande Comore volcanics: melting processes in an upwelling plume. *Earth Planet.*  
3 *Sci. Lett.* 164, 119-133.

4 Camus, G., Gourgaud, A., Mossand-Berthommier, P.C., Vincent, P.M., 2000. Merapi (Central  
5 Java, Indonesia): An outline of the structural and magmatological evolution, with a  
6 special emphasis to the major pyroclastic events. *J. Volcanol. Geotherm. Res.* 100, 139-  
7 163.

8 Carn, S.A., Pyle, D.M., 2001. Petrology and geochemistry of the Lamongan Volcanic Field,  
9 East Java, Indonesia: Primitive Sunda Arc magmas in an extensional tectonic setting? *J.*  
10 *Petrol.* 42, 1643-1683.

11 Charlier, B.L.A., Ginibre, C., Morgan, D., Nowell, G.M., Pearson, D.G., Davidson, J.P.,  
12 Ottley, C.J., 2006. Methods for the microsampling and high-precision analysis of  
13 strontium and rubidium isotopes at single crystal scale for petrological and  
14 geochronological applications. *Chem. Geol.* 232, 114-133.

15 Chauvel, C., Blichert-Toft, J., 2001. A hafnium isotope and trace element perspective on  
16 melting of the depleted mantle. *Earth Planet. Sci. Lett.* 190, 137-151.

17 Conrad, W.K., Kay, S.M., Kay, R.W., 1983. Magma mixing in the Aleutian Arc: evidence  
18 from cognate inclusions and composite xenoliths. *J. Volcanol. Geotherm. Res.* 18, 279-  
19 295.

20 Curray, J.R., Shor Jr, G.G., Raitt, R.W., Henry, M., 1977. Seismic refraction and reflection  
21 studies of crustal structure of the eastern Sunda and western Banda arcs. *J. Geophys.*  
22 *Res.* 82, 2479-2489.

23 Davidson, J.P., 1987. Crustal contamination versus subduction zone enrichment: examples  
24 from the Lesser Antilles and implications for mantle source compositions of island arc  
25 volcanic rocks. *Geochim. Cosmochim. Acta* 51, 2185-2198.

- 1 Davidson, J.P., Dungan, M.A., Ferguson, K.M., Colucci, M.T., 1987. Crust-magma  
2 interactions and the evolution of arc magmas: The San Pedro-Pellado volcanic complex,  
3 southern Chilean Andes. *Geology* 15, 443-446.
- 4 Davidson, J.P., Harmon, R.S., 1989. Oxygen isotope constraints on the petrogenesis of  
5 volcanic arc magmas from Martinique, Lesser Antilles. *Earth Planet. Sci. Lett.* 95, 255-  
6 270.
- 7 Davidson, J.P., Hora, J.M., Garrison, J.M., Dungan, M.A., 2005. Crustal forensics in arc  
8 magmas. *J. Volcanol. Geotherm. Res.* 140, 157-170.
- 9 Davidson, J., Turner, S., Handley, H., Macpherson, C., Dosseto, A., 2007. Amphibole  
10 "sponge" in arc crust? *Geology*.35, 787-790.
- 11 Davidson, J.P., Wilson, I.R., 1989. Evolution of an alkali basalt-trachyte suite from Jebel  
12 Marra volcano, Sudan, through assimilation and fractional crystallization. *Earth Planet.*  
13 *Sci. Lett.* 95, 141-160.
- 14 de Hoog, J.C.M., Taylor, B.E., van Bergen, M.J., 2001. Sulfur isotope systematics of basaltic  
15 lavas from Indonesia: implications for the sulfur cycle in subduction zones. *Earth*  
16 *Planet. Sci. Lett.* 189, 237-252.
- 17 de Hoog, J.C.M., Koetsier, G.W., Bronto, S., Sriwana, T., Van Bergen, M.J., 2001. Sulfur and  
18 chlorine degassing from primitive arc magmas: Temporal changes during the 1982-1983  
19 eruptions of Galunggung (West Java, Indonesia). *J. Volcanol. Geotherm. Res.* 108, 55-  
20 83.
- 21 DeMets, C., Gordon, R.G., Argus, D.F., Stein, S., 1990. Current plate motions. *Geophysical*  
22 *Journal International* 101, 425-478.
- 23 DePaolo, D.J., 1981. Trace element and isotopic effects of combined wallrock assimilation  
24 and fractional crystallization. *Earth Planet. Sci. Lett.* 53, 189-202.

- 1 Dowall, D.P, Nowell, G.M., Pearson, D.G., 2003. Chemical pre-concentration procedures for  
2 high-precision analysis of Hf-Nd-Sr isotopes in geological materials by plasma  
3 ionisation multi-collector mass spectrometry (PIMMS) techniques. *Plasma Source Mass  
4 Spectrometry. Spec. Pub. Royal Society of Chemistry*, 321-337.
- 5 Edwards, C.M.H., 1990. Petrogenesis of tholeiitic, calc-alkaline and alkaline volcanic rocks,  
6 Sunda arc, Indonesia. Unpublished Ph.D. Thesis, Royal Holloway, University of  
7 London, UK.
- 8 Elburg, M., Foden, J., van Bergen, M.J, Zulkarnain, I., 2005. Australia and Indonesia in  
9 collision: geochemical sources of magmatism. *J. Volcanol. Geotherm. Res.* 140, 25-47.
- 10 Elliot, T.R., Plank T., Zindler A., White W., Bourdon B., 1997. Element transport from slab  
11 to volcanic front at the Mariana Arc. *J. Geophys. Res.* B102 14991-15019
- 12 Ewart, A., 1982. The mineralogy and petrology of Tertiary-Recent orogenic volcanic rocks:  
13 with special reference to the andesitic-basaltic compositional range. In *Andesites:  
14 Orogenic Andesites and Related Rocks*, ed R.S. Thorpe, pp. 525-48. Wiley, Chichester.
- 15 Ewart, A., Bryan, W. B., Chappell, B. W., Rudnick, R. L., 1994. Regional geochemistry of  
16 the Lau-Tonga arc and back-arc systems. *Proc. Ocean Drilling Program, Scientific  
17 Results* 135, 385-425.
- 18 Flood, T.P., Schuraytz, B.C., Vogel, T.A., 1989. Magma mixing due to disruption of a layered  
19 magma body. *J. Volcanol. Geotherm. Res.* 36, 241-255.
- 20 Gamble, J.A., Smith, I.E.M., McCulloch, M.T., Graham, I.J., Kokelaar, B.P., 1993. The  
21 geochemistry and petrogenesis of basalts from the Taupo volcanic zone and Kermadec  
22 island arc, S.W. Pacific. *J. Volcanol. Geotherm. Res.* 54, 265-290.
- 23 Gasparon, M., 1993. Origin and evolution of mafic volcanics of Sumatra (Indonesia): their  
24 mantle sources, and roles of subducted oceanic sediments and crustal contamination.  
25 Unpublished Ph.D. Thesis, Univ. Tasmania.

- 1 Gasparon, M., Hilton, D. R., Varne, R., 1994. Crustal contamination processes traced by  
2 helium isotopes: Examples from the Sunda arc, Indonesia. *Earth Planet. Sci. Lett.* 126,  
3 15-22.
- 4 Gasparon, M., Varne, R., 1998. Crustal assimilation versus subducted sediment input in west  
5 Sunda arc volcanics: an evaluation. *Mineralogy and Petrology* 64, 89-117.
- 6 Gerbe, M.-C., Gouraud, A., Sigmarsson, O., Harmon, R.S., Joron, J-L., Provost, A., 1992.  
7 Mineralogical and geochemical evolution of the 1982-1983 Galunggung eruption  
8 (Indonesia). *Bulletin of Volcanology* 54, 284-298.
- 9 GERM: <http://earthref.org/GERM/index.html>
- 10 Gertisser, R., Keller, J., 2003a. Trace element and Sr, Nd, Pb and O isotope variations in  
11 medium-K and high-K volcanic rocks from Merapi Volcano, Central Java, Indonesia:  
12 evidence for the involvement of subducted sediments in Sunda Arc magma genesis. *J.*  
13 *Petrol.* 44, 457-489.
- 14 Gertisser, R., Keller, J., 2003b. Temporal variations in magma composition at Merapi  
15 Volcano (Central Java, Indonesia): magmatic cycles during the past 2000 years of  
16 explosive activity. *J. Volcanol. Geotherm. Res.* 123, 1-23.
- 17 Gill, J.B., 1981. *Orogenic Andesites and Plate Tectonics*. Springer, Berlin.
- 18 Grove, T.L., Baker, M.B., Price, R.C., Parman, S.W., Elkins-Tanton, L.T., Chatterjee, N.,  
19 Muntener, O., 2005. Magnesian andesite and dacite lavas from Mt. Shasta, northern  
20 California: products of fractional crystallisation of H<sub>2</sub>O-rich mantle melts. *Contrib.*  
21 *Mineral. Petrol.* 148, 542-565.
- 22 Hamilton, W.B., 1979. *Tectonics of the Indonesian region*. U.S. Geological Survey  
23 Professional Paper reprinted with corrections, 1981 and 1985, 1078: 345.

- 1 Handley, H.K., 2006. Geochemical and Sr-Nd-Hf-O isotopic constraints on volcanic  
2 petrogenesis at the Sunda arc, Indonesia. Unpublished Ph.D. Thesis, Durham  
3 University, UK.
- 4 Handley, H.K., Macpherson, C.G., Davidson, J.P., Berlo, K., Lowry, D., 2007. Constraining  
5 fluid and sediment contributions to subduction-related magmatism in Indonesia: Ijen  
6 Volcanic Complex, Indonesia. *J. Petrol.* 48, 1155-1183.
- 7 Harmon, R.S., Gerbe, M.C., 1992. The 1982-83 eruption at Galunggung volcano, Java  
8 (Indonesia): oxygen isotope geochemistry of a zoned magma chamber. *J. Petrol.* 33,  
9 585-609.
- 10 Hildreth, W., Moorbath, S., 1988. Crustal contributions to arc magmatism in the Andes of  
11 Central Chile. *Contrib. Mineral. Petrol.* 98, 455-489.
- 12 Ionov, D.A., Harmon, R.S., France-Lanord, C., Greenwood, B., Ashchepkov, I.V., 1994.  
13 Oxygen isotope composition of garnet and spinel peridotites in the continental mantle:  
14 Evidence from the Vitim xenolith suite, southern Siberia. *Geochim. Cosmochim. Acta*,  
15 58, 1463-1470.
- 16 Ito, E., White, W.M., Gopel, C., 1987. The O, Sr, Nd and Pb isotope geochemistry of MORB.  
17 *Chem. Geol.* 62, 157-176.
- 18 Jarrard, R.D., 1986. Relations among subduction parameters. *Rev. Geophys.* 24, 217-284.
- 19 Kadarusman, A., Miyashita, S., Maruyama, S., Parkinson, C.D., Ishikawa, A., 2004.  
20 Petrology, geochemistry and paleogeographic reconstruction of the East Sulawesi  
21 Ophiolite, Indonesia. *Tectonophysics* 392, 55-83.
- 22 Kieckhefer, R.M., Shor Jr, G.G., Curray, J.R., 1980. Seismic refraction studies of the Sunda  
23 trench and forearc basin. *J. Geophys. Res.* 85, 863-889.
- 24 Langmuir, C.H., Voche, R.D., Hanson, G.N., Hart, S.R., 1978. A general mixing equation  
25 with applications to Icelandic basalts. *Earth Planet. Sci. Lett.* 37, 380-392.

- 1 Le Pichon, X., 1968. Sea-floor spreading and continental drift. *J. Geophys. Res.* 73, 3661-  
2 3697.
- 3 Macpherson, C.G., Hilton, D.R., Matthey, D.P., Sinton, J.M., 2000. Evidence for an  $^{18}\text{O}$ -  
4 depleted mantle plume from contrasting  $^{18}\text{O}/^{16}\text{O}$  ratios of back-arc lavas from the Manus  
5 Basin and Mariana Trough. *Earth Planet. Sci. Lett.* 176, 171-183.
- 6 Marcoux, E., Milesi, J-P., 1994. Epithermal gold deposits in West Java, Indonesia: geology,  
7 age and crustal source. *Journal of Geochemical Exploration* 50, 393-408.
- 8 Matthey, D., Lowry, D., Macpherson, C., 1994. Oxygen isotope composition of mantle  
9 peridotite. *Earth Planet. Sci. Lett.* 128, 231-241.
- 10 McCulloch, M.T., Gamble J.A., 1991. Geochemical and geodynamical constraints on  
11 subduction zone magmatism. *Earth Planet. Sci. Lett.* 102, 358-374.
- 12 Nowell, G.M., Kempton, P.D., Noble, S.R., Fitton, J.G., Saunders, A.D., Mahoney, J.J.,  
13 Taylor, R.N., 1998. High precision Hf isotope measurements of MORB and OIB by  
14 thermal ionisation mass spectrometry: insights into the depleted mantle. *Chem. Geol.*  
15 149, 211-233.
- 16 Nowell, G.M., Pearson, D.G., Ottley, C.J., Schweiters, J., 2003. Long-term performance  
17 characteristics of a plasma ionisation multi-collector mass spectrometer (PIMMS): the  
18 ThermoFinnigan Neptune. *Plasma Source Mass Spectrometry. Spec. Pub. Royal Society*  
19 *of Chemistry*, 307-320.
- 20 Ottley, C.J., Pearson, D.G., Irvine, G.J., 2003. A routine method for the dissolution of  
21 geological samples for the analysis of REE and trace elements via ICP-MS. *Plasma*  
22 *Source Mass Spectrometry. Spec. Pub. Royal Society of Chemistry*, 221-230.
- 23 Patchett, P.J., 1983. Hafnium isotope results from mid-ocean ridges and Kerguelen. *Lithos* 16,  
24 47-51.

- 1 Patchett, P.J., Tatsumoto, M., 1980. Hafnium isotope variations in oceanic basalts. *Geophys.*  
2 *Res. Lett.* 7, 1077-1080.
- 3 Pearce, J.A., 1982. Trace element characteristics of lavas from destructive plate boundaries.  
4 *Andesites: Orogenic Andesites and Related Rocks.* John Wiley & Sons, Chichester, UK,  
5 525-548.
- 6 Pearce, J.A., Kempton, P.D., Nowell, G.M., Noble, S.R., 1999. Hf-Nd Element and Isotope  
7 Perspective on the Nature and Provenance of Mantle and Subduction Components in  
8 Western Pacific Arc-Basin Systems. *J. Petrol.* 40, 1579-1611.
- 9 Price, R.C., Kennedy, A.K., Riggs-Sneeringer, M., Frey, F.A., 1986. Geochemistry of basalts  
10 from the Indian Ocean triple junction: implications for the generation and evolution of  
11 Indian Ocean ridge basalts. *Earth Planet. Sci. Lett.* 78, 379-396.
- 12 Rapp, R.P., Watson, E.B., 1995. Dehydration melting of a metabasalt at 8-32 kbar:  
13 Implications for continental growth and crustal recycling. *J. Petrol.* 36, 891-931.
- 14 Rehkämper, M., Hofmann, A.W., 1997. Recycled ocean crust and sediment in Indian Ocean  
15 MORB. *Earth Planet. Sci. Lett.* 147, 93-106.
- 16 Reubi, O., Nicholls, I.A., 2004. Magmatic evolution at Batur volcanic field, Bali, Indonesia:  
17 petrological evidence for polybaric fractional crystallisation and implications for  
18 caldera-forming eruptions. *J. Volcanol. Geotherm. Res.* 138, 345-369.
- 19 Reubi, O., Nicholls, I.A., Kamenetsky, V.S., 2002. Early mixing and mingling in the  
20 evolution of basaltic magmas: evidence from phenocryst assemblages, Slamet Volcano,  
21 Java, Indonesia. *J. Volcanol. Geotherm. Res.* 119, 255-274.
- 22 Royse, K., Kempton, P.D., Darbyshire, D.P.F., 1998. NERC Isotope Geosciences Laboratory  
23 Report Series, 121.
- 24 Salters, V.J.M., 1996. The generation of mid-ocean ridge basalts from the Hf and Nd isotope  
25 perspective. *Earth Planet. Sci. Lett.* 141, 109-123.

1     Salters, V.J.M., Hart, S.R., 1991. The mantle sources of ocean islands and arc basalts: the Hf  
2           isotope connection. *Earth Planet. Sci. Lett.* 104, 364-380.

3     Salters, V.J.M., White, W.M., 1998. Hf isotope constraints on mantle evolution. *Chem. Geol.*  
4           145, 447-460.

5     Sitorus, K., 1990. Volcanic stratigraphy and geochemistry of the Idjen Caldera Complex, East  
6           Java, Indonesia, MSc thesis, University of Wellington, New Zealand.

7     Staudigel, H., Plank, T., White, B., Schimincke, H-U., 1996. Geochemical fluxes during  
8           seafloor alteration of the basaltic upper oceanic crust: DSDP Sites 417 and 418,  
9           Subduction: Top to Bottom. *Geophysical Monograph* 96, pp. 19-36.

10    Stille, P., Unruh, D.M., Tatsumoto, M., 1986. Pb, Sr, Nd, and Hf isotopic constraints on the  
11          origin of Hawaiian basalts and evidence for a unique mantle source. *Geochim.*  
12          *Cosmochim. Acta* 50, 2303-2319.

13    Stimac, J., 2003. Surface geology of the Awibengkok geothermal development area, Java,  
14          Indonesia. Unocal report, Philippines.

15    Stormer, J. C., Jr., Nicholls, J., 1978. XLFRAC; a program for the interactive testing of  
16          magmatic differentiation models. *Computers & Geosciences* 4, 143-159.

17    Sun, S., McDonough, W.F., 1989. Chemical and isotopic systematics of oceanic basalts:  
18          implications for mantle composition and processes. In: A.D. Saunders, Norry, M.J.  
19          (Editor), *Magmatism in the Ocean Basins*. Geological Society Special Publication, 313-  
20          345.

21    Taylor, S.R., 1977. Island arc models and the composition of the continental crust, in  
22          Talwani, M., Pitman, W., eds., *Island arcs, deep sea trenches and back arc basins*:  
23          American Geophysical Union, Maurice Ewing Series 1, 325-335.

- 1 Tepley, F.J., III, Davidson, J.P., Tilling, R.I., Arth, J.G., 2000. Magma mixing, recharge and  
2 eruption histories recorded in plagioclase phenocrysts from El Chichon, Mexico. *J.*  
3 *Petrol.* 41, 1397-1411.
- 4 Thirlwall, M.F., 1991. Long-term reproducibility of multicollector Sr and Nd isotope ratio  
5 analysis. *Chem. Geol.; Isotope Geoscience Section* 94, 85-104.
- 6 Thirlwall, M.F., Graham A.M., Arculus R.J., Harmon R.S., Macpherson C.G., 1996.  
7 Resolution of the effect of crustal assimilation, sediment subduction and fluid transport  
8 in island arc magmas: Pb-Sr-Nd-O isotope geochemistry of Grenada, Lesser Antilles.  
9 *Geochim. Cosmochim. Acta* 60, 4785-4810.
- 10 Tregoning, P., Brunner, F.K., Bock, Y., Puntodewo, S.S.O., McCaffrey, R., Genrich, J.F.,  
11 Calais, E., Rais, J., Subarya, C., 1994. First geodetic measurement of convergence  
12 across the Java Trench. *Geophys. Res. Lett.* 21, 2135-2138.
- 13 Turner, S., Foden, J., George, R., Evans, P., Varne, R., Elburg, M., Jenner, G., 2003. Rates and  
14 processes of potassic magma evolution beneath Sangeang Api volcano, East Sunda Arc,  
15 Indonesia. *J. Petrol.* 44, 491-515.
- 16 Turner, S., Hawkesworth, C., Rogers, N., Bartlett, J., Worthington, T., Hergt, J., Pearce, J.,  
17 Smith, I., 1997.  $^{238}\text{U}$ - $^{230}\text{Th}$  disequilibria, magma petrogenesis and flux rates beneath the  
18 depleted Tonga-Kermadec island arc. *Geochim. Cosmochim. Acta* 61, 4855-4884.
- 19 van Gerven, M., Pichler, H., 1995. Some aspects of the volcanology and geochemistry of the  
20 Tengger Caldera, Java, Indonesia: eruption of a K-rich tholeiitic series. *Journal of*  
21 *Southeast Asian Earth Sciences* 11, 125-133.
- 22 Vervoort, J.D., Patchett, P.J., Blichert-Toft, J., Albarede, F., 1999. Relationships between Lu-  
23 Hf and Sm-Nd isotopic systems in the global sedimentary system. *Earth Planet. Sci.*  
24 *Lett.* 168, 79-99.

- 1 Vogel, T.A., 1982. Magma mixing in the acidic-basic complex of Ardnamurchan;  
2 implications on the evolution of shallow magma chambers. *Contrib. Mineral. Petrol.* 79,  
3 411-423.
- 4 Vukadinovic, D., Sutawidjaja, I., 1995. Geology, mineralogy and magma evolution of  
5 Gunung Slamet Volcano, Java, Indonesia. *Journal of Southeast Asian Earth Sciences*,  
6 11, 135-164.
- 7 White, W.M., Patchett, J., 1984. Hf-Nd-Sr isotopes and incompatible element abundances in  
8 island arcs: implications for magma origins and crustal-mantle evolution. *Earth Planet.*  
9 *Sci. Lett.* 67, 167-185.
- 10 White, W.M., Patchett, J., Ben Othman, D., 1986. Hf isotope ratios of marine sediments and  
11 Mn nodules; evidence for a mantle source of Hf in seawater. *Earth Planet. Sci. Lett.* 79,  
12 46-54.
- 13 Whitford, D.J., White, W.M., Jezek, P.A., 1981. Neodymium isotopic composition of  
14 Quaternary island arc lavas from Indonesia. *Geochim. Cosmochim. Acta* 45, 989-995.
- 15 Woodhead, J.D., 1989. Geochemistry of the Mariana Arc (Western Pacific): Source  
16 composition and processes, *Chem. Geol.* 76, 1-24.
- 17 Woodhead, J.D., Eggins, S.M., Gamble, J., 1993. High field strength and transition element  
18 systematics in island arc and back-arc basin basalts: evidence for multi-phase melt  
19 extraction and depleted mantle wedge. *Earth Planet. Sci. Lett.* 114, 491-504.
- 20 Woodhead, J.D., Hergt, J.M., Davidson, J.P., Eggins, S.M., 2001. Hafnium isotope evidence  
21 for 'conservative' element mobility during subduction processes. *Earth Planet. Sci. Lett.*  
22 192, 331-346.
- 23 Zaennudin, A., Sutawidjaja, I.S., Aswin, D., 1993. Geological map of Salak Volcano, West  
24 Java. Volcanic Survey of Indonesia, Indonesia.

1 Zellmer G.F., Hawkesworth, C.J., Sparks, R.S.J., Thomas, L.E., Harford, C.L., Brewer, T.S.,  
2 Loughlin, S.C., 2003. Geochemical evolution of the Soufriere Hills Volcano,  
3 Montserrat, Lesser Antilles Volcanic Arc. *J. Petrol.* 44, 1349-1374.

4

## 5 **Figure Captions**

6 Fig. 1. Topographic sketch map of the Salak-Perbakti-Gagak Complex, showing the  
7 distribution of samples used in this study and corresponding data symbols used on subsequent  
8 figures. CVG = Central Vent Group; SVG = Side Vent Group; SL3 = Salak lava 3 (Zaennudin  
9 et al., 1993). Selected rivers are shown in black dash; solid lines with ticks represent  
10 escarpments. Inset diagram shows the location of Salak (large black triangle) in West Java, in  
11 relation to major centres of population (grey fill) and Quaternary volcanoes (small black  
12 triangles).

13

14 Fig. 2. Analyses of pyroxene phenocrysts in Salak lavas. Dashed lines represent 10%  
15 increments.

16

17 Fig. 3. Compositional variation of plagioclase phenocrysts in Salak volcanic rocks. Grey lines  
18 represent 10% increments.

19

20 Fig. 4. Major element variation diagrams for Salak volcanic rocks. Tengger Caldera (open  
21 circles) distinguished from the other Java volcanic data (small crosses) to highlight the  
22 unusual geochemical properties of the rocks (data from van Gerven & Pichler, 1995). Java  
23 data: B, Bayah Dome (Marcoux and Milesi, 1994; Alves et al., 1999); C, Cereme (Edwards,  
24 1990); G, Gede Volcanic Complex (Handley, 2006); Ga, Galunggung (Gerbe et al., 1992; de  
25 Hoog et al., 2001); Gu, Guntur (Edwards, 1990; de Hoog et al., 2001); I, Ijen Volcanic

1 Complex (Handley et al., 2007); M, Merapi (Gertisser and Keller, 2003a); S, Slamet  
2 (Vukadinovic and Sutawidjaja, 1995; Reubi and Nicholls, 2002). Model fractionation curves  
3 are shown for removal of the mineral assemblage suggested by least squares modelling from  
4 S106B (model 1) in Table 9: 0.7 Plag, 0.1 Cpx, 0.13 Opx, 0.07 Fe-Ti oxide. Mineral data used  
5 in modelling is given in Tables 3-5. Fractionation curves are labelled with the percentage of  
6 melt remaining.

7

8 Fig. 5. Selected trace element variations with SiO<sub>2</sub> for Salak volcanic rocks. Java data sources  
9 as in Fig. 4. SVG samples erupted from eastern flank (E. Flank) and western flank (W. Flank)  
10 vents are indicated in b). Model fractionation curves (FC) are shown for 100% amphibole  
11 fractionation (crosses) from Javan basalt (Ijen Volcanic Complex KI69, Handley et al., 2007)  
12 using mineral partition coefficients from Bottazzi et al. (1999) and mineral composition from  
13 Rapp and Watson at 8kbar, 1000°C (1995), and for fractionation of the mineral assemblage  
14 suggested by least squares modelling (horizontal ticks) see Fig. 4 for details. Curves are  
15 labelled with the percentage of melt remaining.

16

17 Fig. 6. Chondrite normalised rare earth element diagram of Salak rocks. Normalising factors  
18 and Normal (N)-MORB values from Sun and McDonough (1989). Indian (I)-MORB  
19 (Chauvel and Blichert-Toft, 2001).

20

21 Fig. 7. Variation of <sup>143</sup>Nd/<sup>144</sup>Nd with <sup>87</sup>Sr/<sup>86</sup>Sr for Salak volcanic rocks. Data sources: I-  
22 MORB: Rehkämper and Hofmann, 1997; Ito et al., 1987; Price et al., 1986; Chauvel and  
23 Blichert-Toft, 2001; N-MORB: Ito et al., 1987; Chauvel and Blichert-Toft, 2001; Java: White  
24 and Patchett, 1984; Whitford et al, 1981; Edwards, 1990; Gertisser and Keller, 2003a; Gerbe  
25 et al, 1992; Handley et al., 2007; Handley, 2006; Indian ocean sediments: Ben Othman et al.,

1 1989; Gasparon and Varne, 1998. Inset: Nd and Sr isotope ratio diagram separated by group.  
2  $2\sigma$  external errors shown for each analysis. E. Flank = eastern flank vent samples S102 and  
3 S103.

4  
5 Fig. 8.  $^{176}\text{Hf}/^{177}\text{Hf}$  -  $^{143}\text{Nd}/^{144}\text{Nd}$  variation in Salak volcanic rocks. Data sources: I-MORB:  
6 Salters, 1996; Nowell et al., 1998; Chauvel and Blichert-Toft, 2001; N-MORB: I-MORB refs.  
7 and Salters and Hart, 1991; OIB: Salters and Hart, 1991; Salters and White, 1998; Nowell et  
8 al., 1998; Patchett and Tatsumoto, 1980; Patchett, 1983; Stille et al., 1986; Java: White and  
9 Patchett, 1983; Woodhead et al., 2001; Handley et al., 2007; Handley, 2006; Banda: White  
10 and Patchett, 1984; Indian ocean sediments: Ben Othman et al., 1989; White et al., 1986;  
11 Vervoort et al., 1999. Dividing line for Indian and Pacific MORB provenance from Pearce et  
12 al., 1999. Inset: Hf-Nd isotope diagram of Salak volcanic rocks separated by group.  $2\sigma$   
13 external errors shown for each analysis on the inset diagram. E. Flank = eastern flank vent  
14 samples S102 and S103.

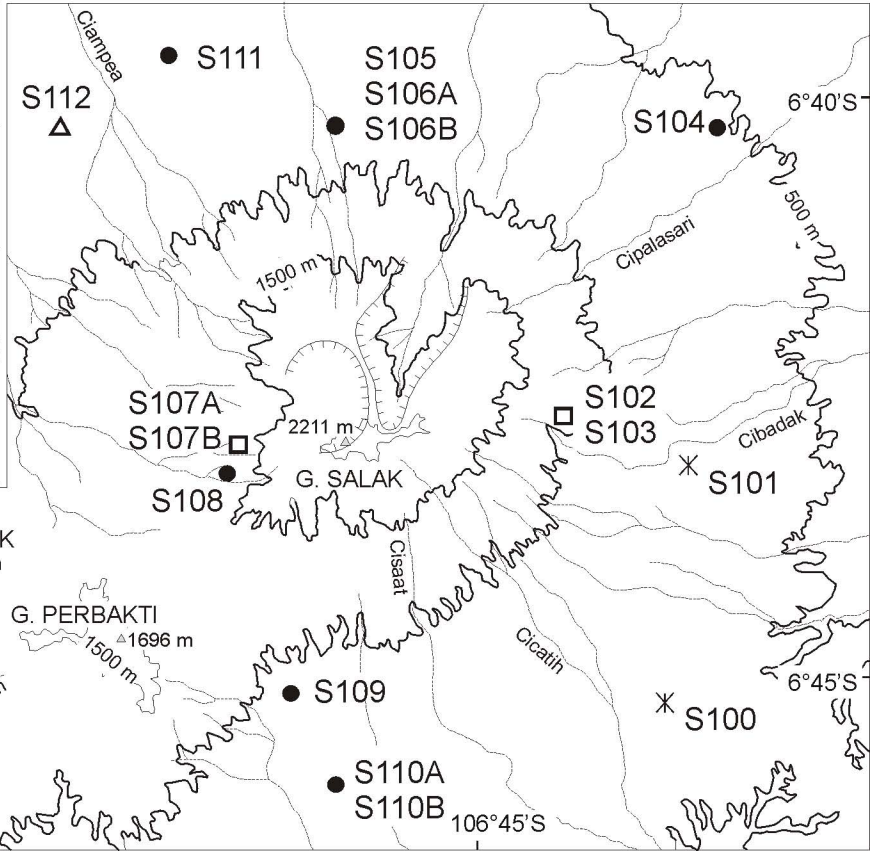
15  
16 Fig. 9. a) K/Rb-Rb and b) Ba/Th-Y, showing fractional crystallisation (FC), combined  
17 assimilation and fractional crystallisation (AFC A, B and C), and bulk mixing (MM A, B, C  
18 and D) curves for models involving Salak basaltic andesite S106B and A: rhyolite (this  
19 study), B & D: Seputih granite plutonics 75415 and 75413 respectively (southern Sumatra,  
20 Gasparon, 1993) and C: Javan arc tholeiite from Guntur, GU1/T (Edwards, 1990). See Table  
21 8 for end member compositions. Tick marks on FC and AFC curves indicate the percentage of  
22 liquid remaining. Tick marks on mixing curves represent the percentage of A, B, C or D  
23 mixed with the magma. FC and AFC calculations use the mineral proportions suggested by  
24 least squares major element modelling of CVG rocks S106B to S110B (Table 9, model 1):  
25 Plag = 0.7; Cpx = 0.1; Opx = 0.13; Oxide = 0.07. AFC curves calculated using DePaolo

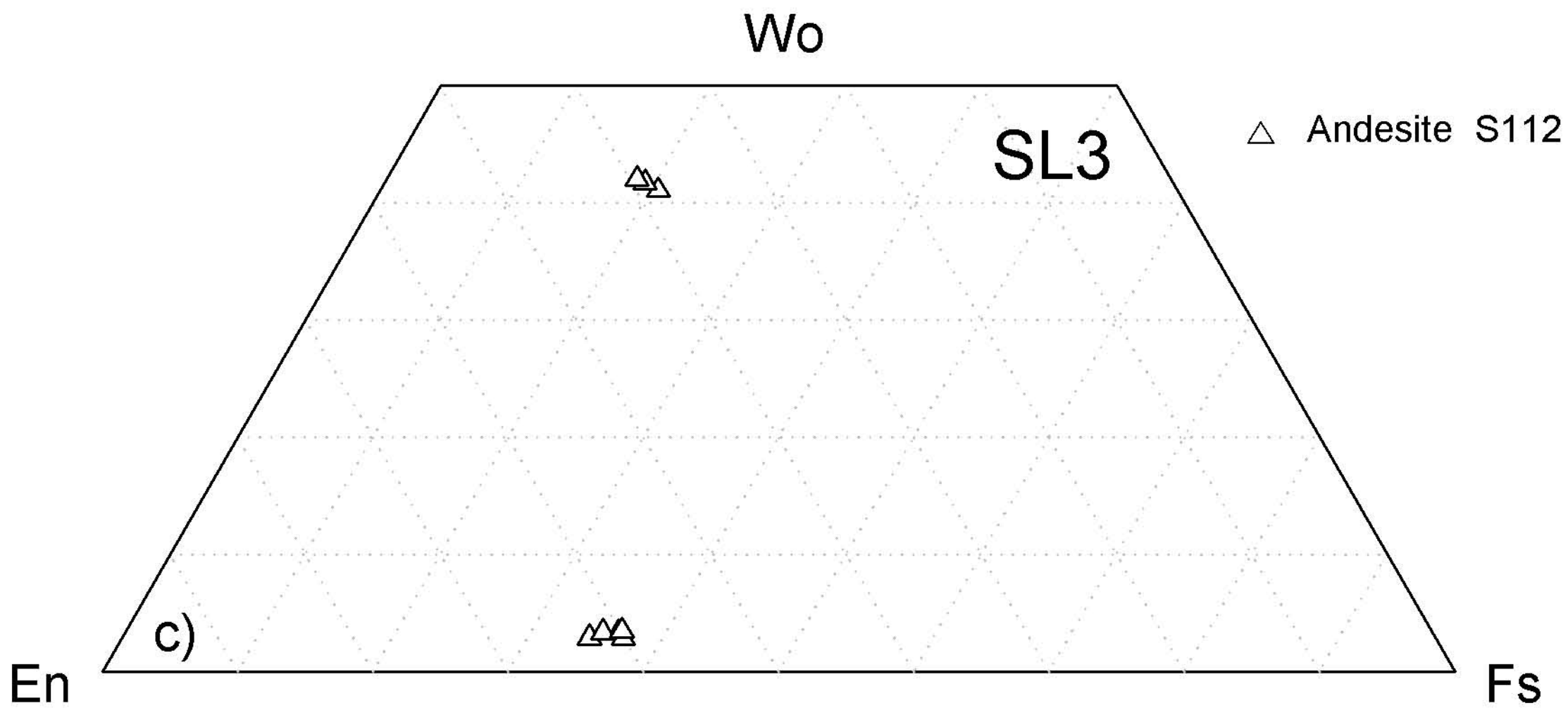
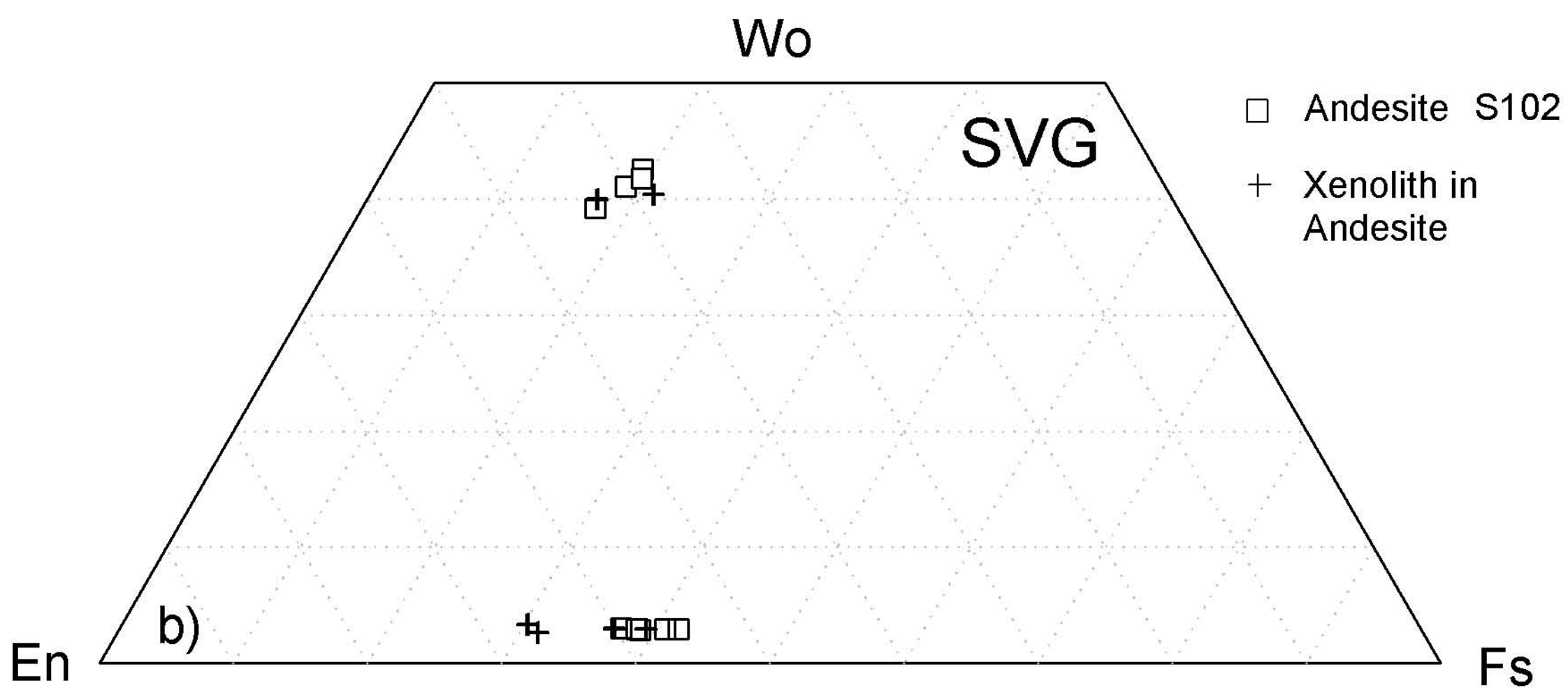
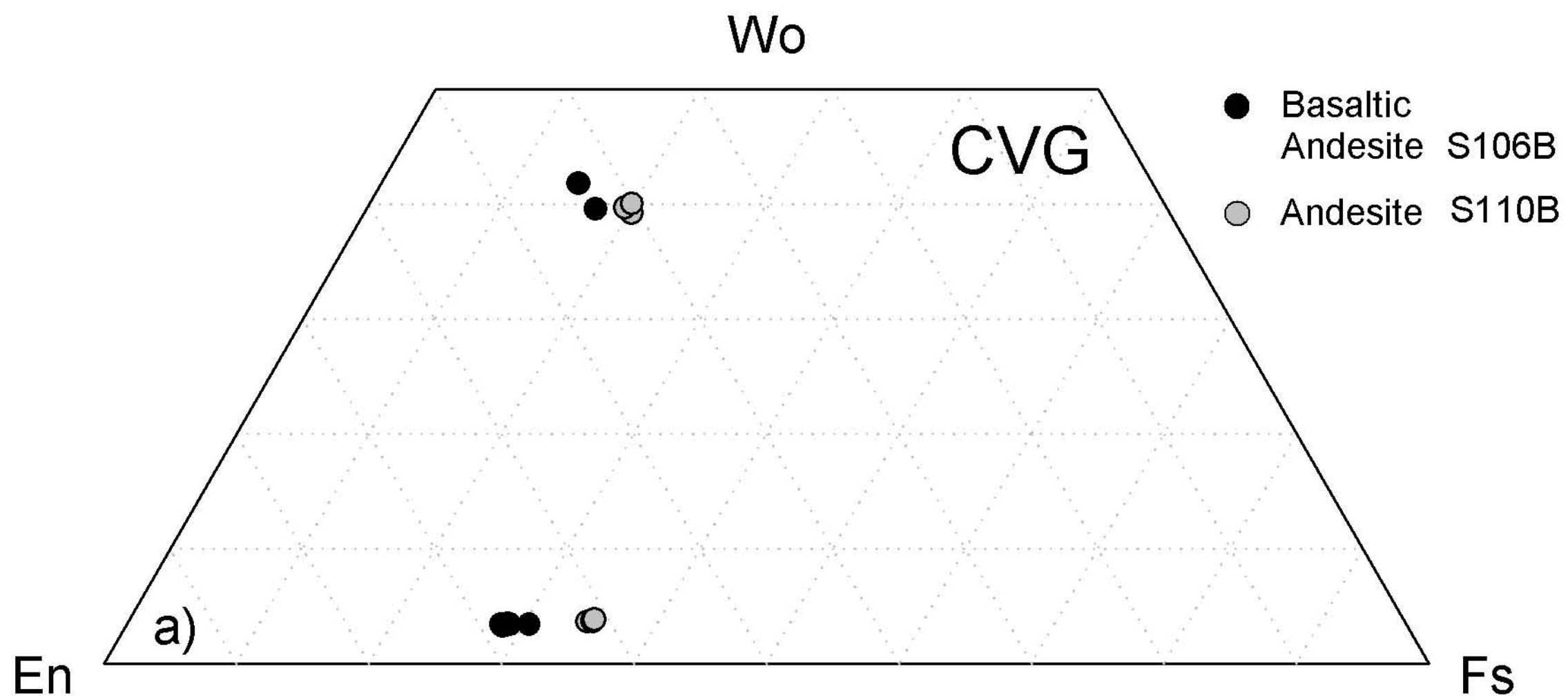
1 (1981). The rate ratio ( $r$ ) of mass assimilated to mass crystallised in AFC model:  $A = 0.5$ ,  $B =$   
2  $0.05$ ,  $C = 0.8$ .

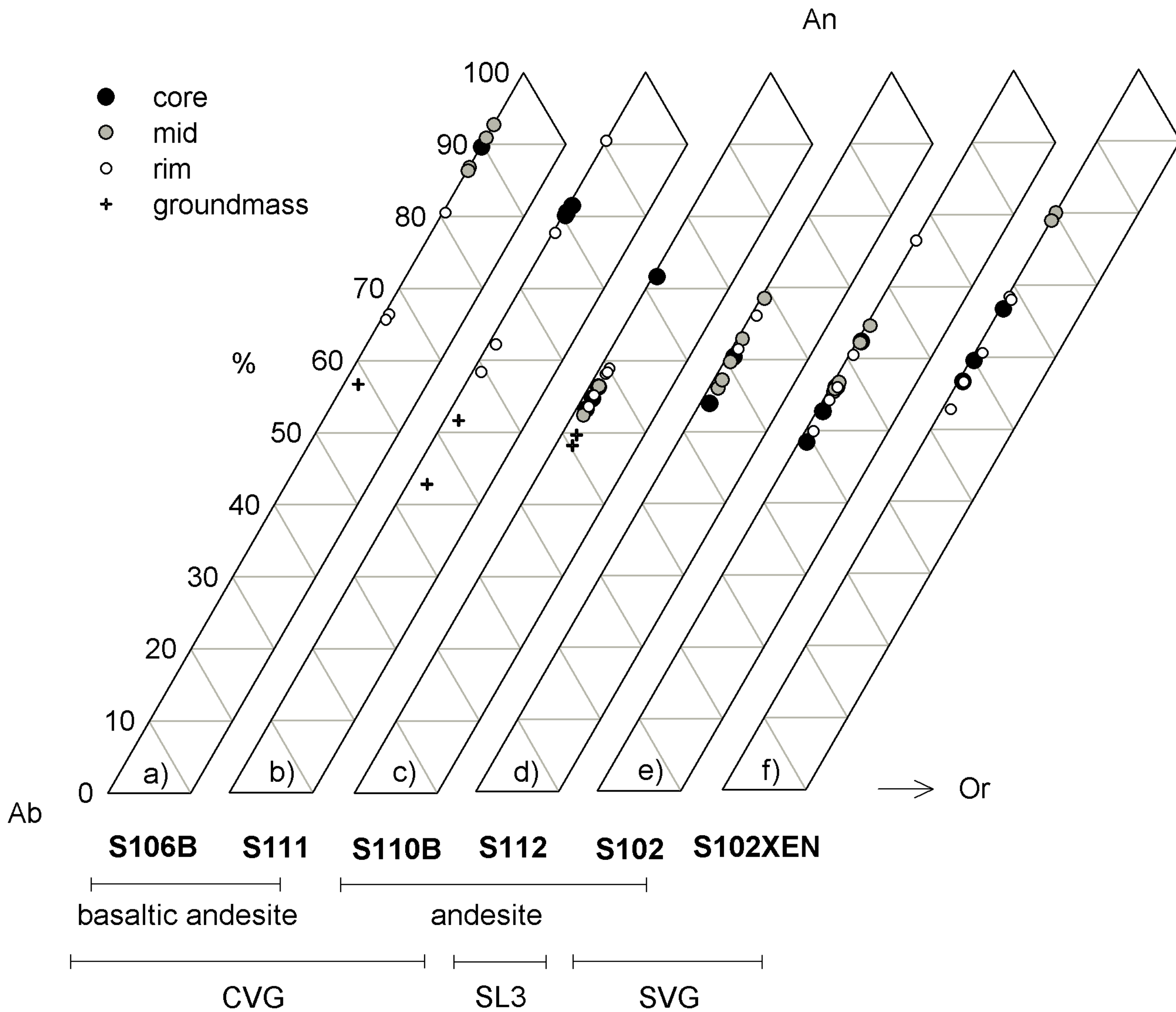
3  
4 Fig. 10. Variation of  $^{87}\text{Sr}/^{86}\text{Sr}$  isotope ratio versus  $\text{SiO}_2$  for Salak volcanic rocks. Arrows  
5 labelled SH, AFC and FC indicate the hypothesised data trends related to: heterogeneity in the  
6 mantle source (SH), combined assimilation and fractional crystallisation (AFC) and fractional  
7 crystallisation (FC). Inset shows Th/Ba versus  $\text{SiO}_2$  for Salak rocks, highlighting the similar  
8 differentiation patterns between Th/Ba and  $^{87}\text{Sr}/^{86}\text{Sr}$  and suggesting the former, for which  
9 there is more data, might serve as a proxy for isotopic composition.

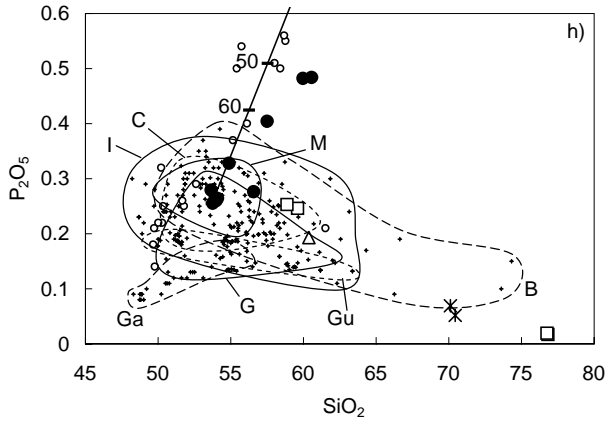
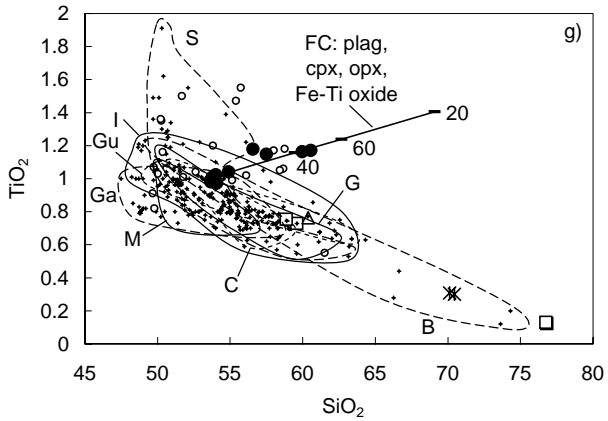
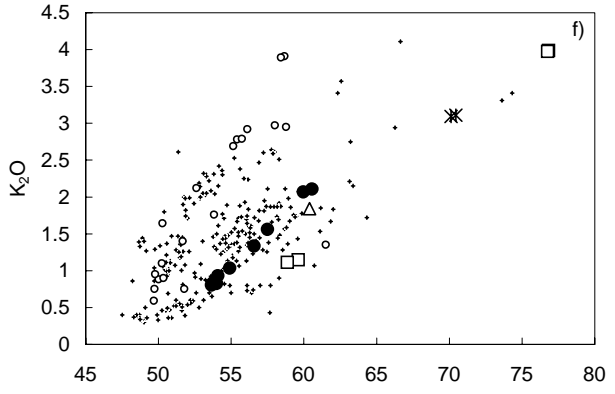
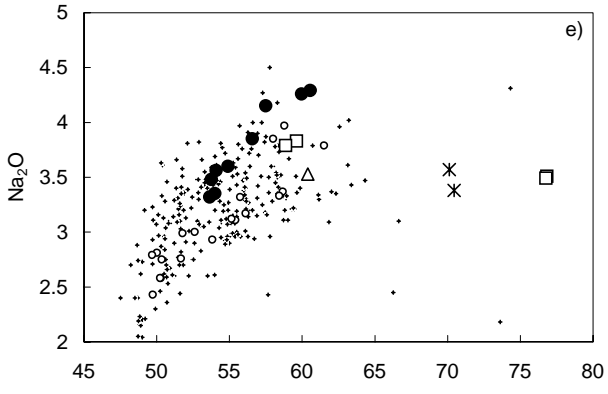
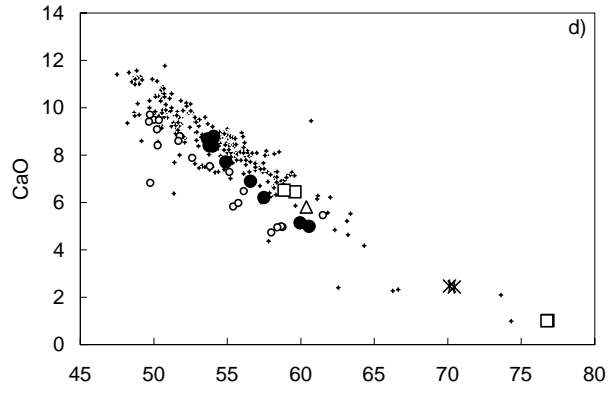
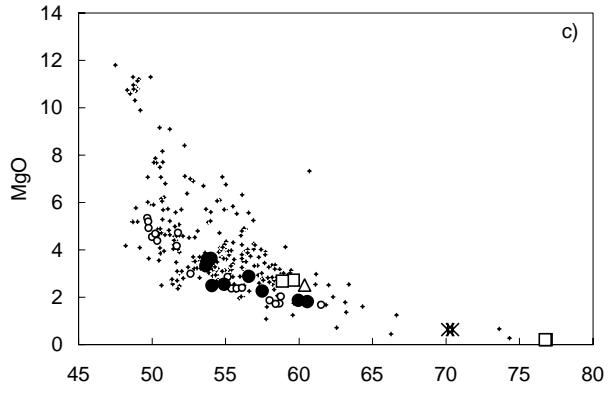
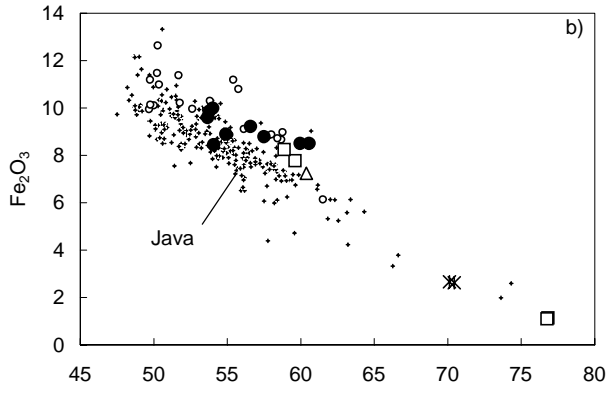
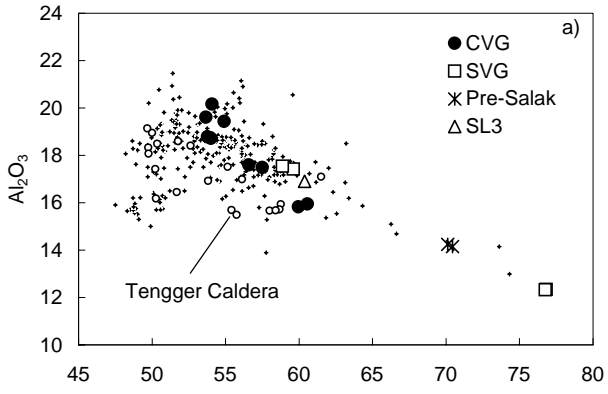
10  
11 Fig. 11. Ba/Th against  $^{87}\text{Sr}/^{86}\text{Sr}$  for Salak volcanic rocks. FC and AFC curves are shown for  
12 the same models (AFC A, B and C) in Fig. 9 (see caption for details).  $^{87}\text{Sr}/^{86}\text{Sr}$  ratios used in  
13 model AFC C is that of GU2/C (Edwards, 1990). Arrow labelled FC indicates differentiation  
14 trend expected from fractional crystallisation alone. Tick marks on FC and AFC curves  
15 indicate the percentage of liquid remaining.

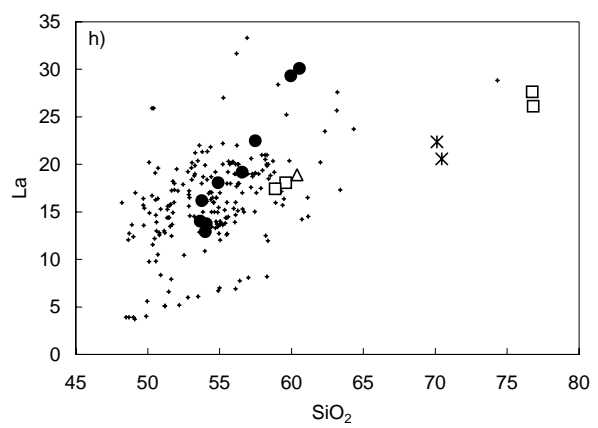
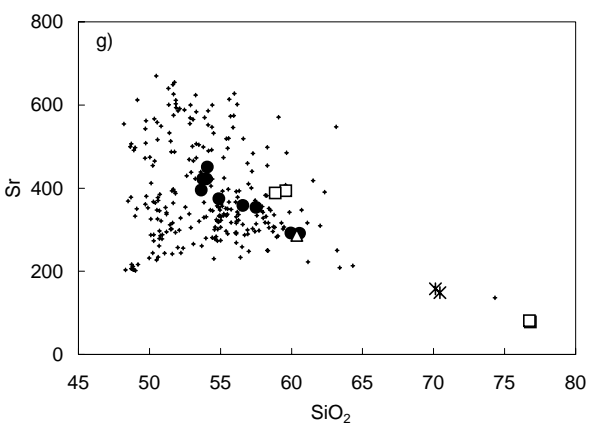
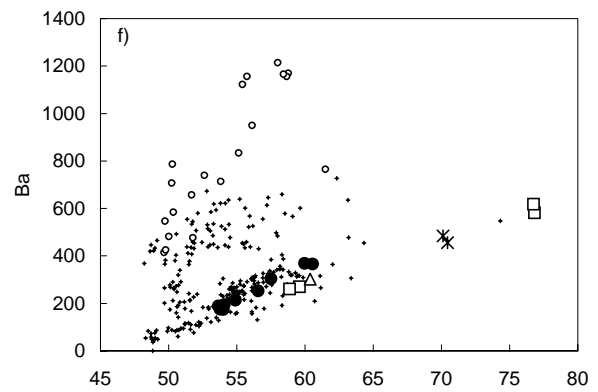
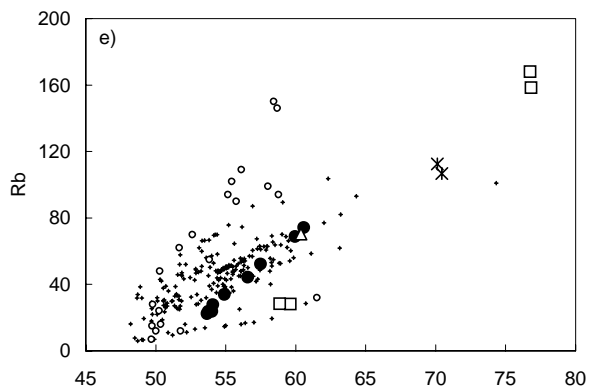
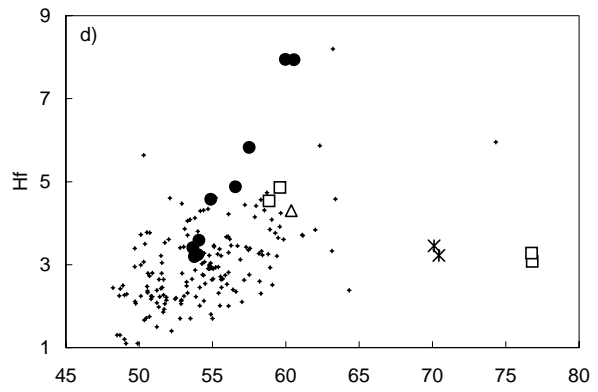
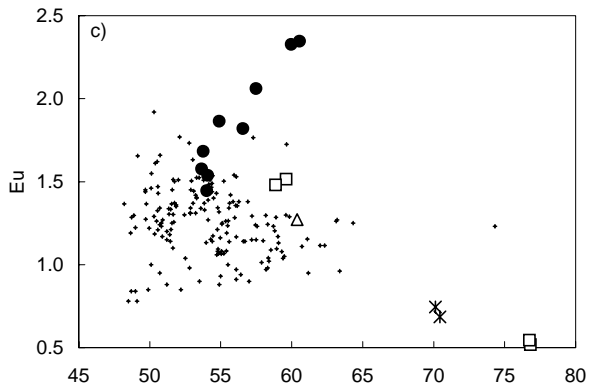
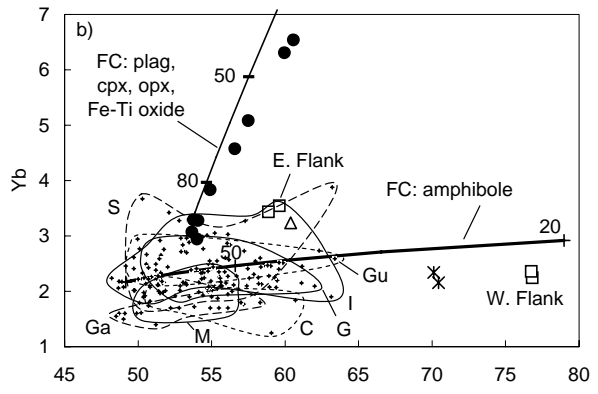
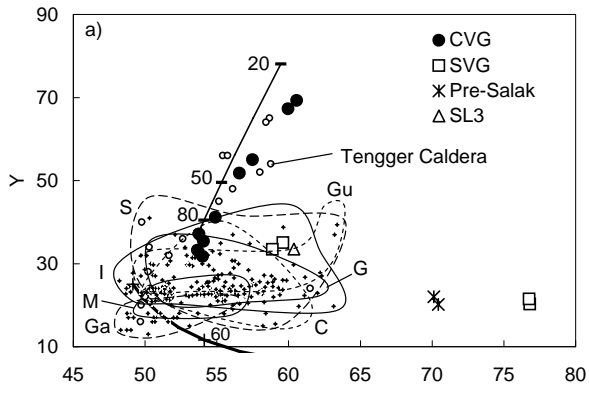
16  
17 Fig. 12. Schematic representation of magmatic evolution, showing the multiple magma  
18 storage areas and pathways envisaged in petrogenesis at Salak. (A) and (B) relate to  
19 discussion in the text: (A) indicates continued magmatic evolution from a CVG-type parent at  
20 shallow depth, involving late-stage fractionation of hornblende in petrogenesis of the western  
21 flank SVG rocks, (B) indicates hypothesised fractionation of a HFSE-HREE compatible  
22 phase at depth in the evolution of SVG magma below the eastern flank vent.

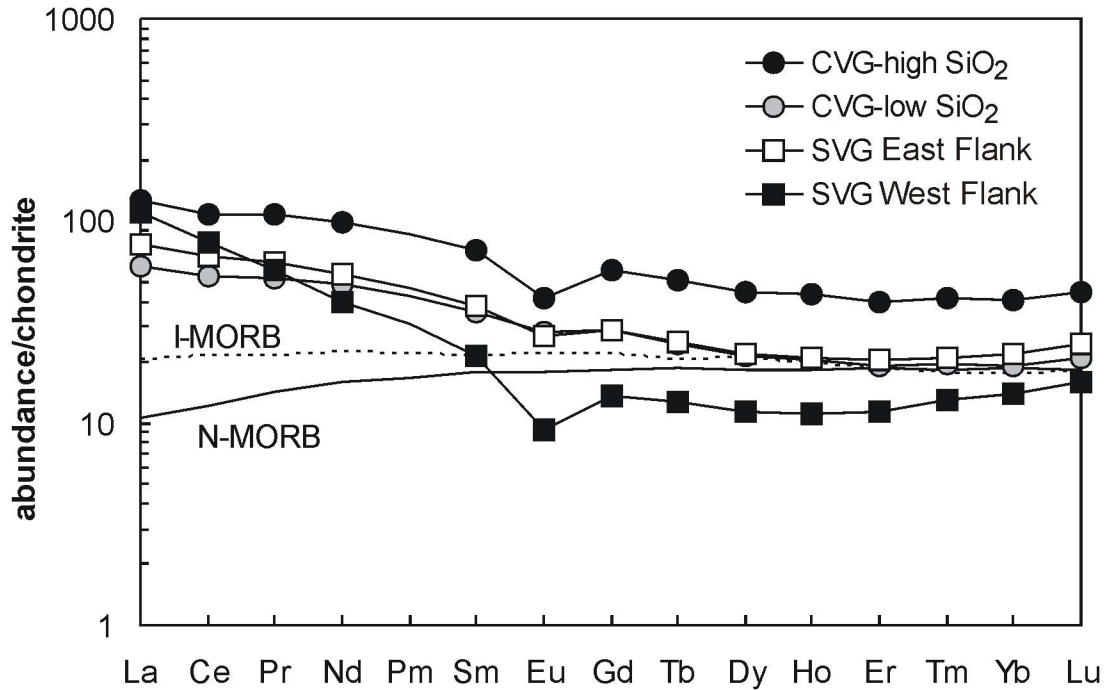


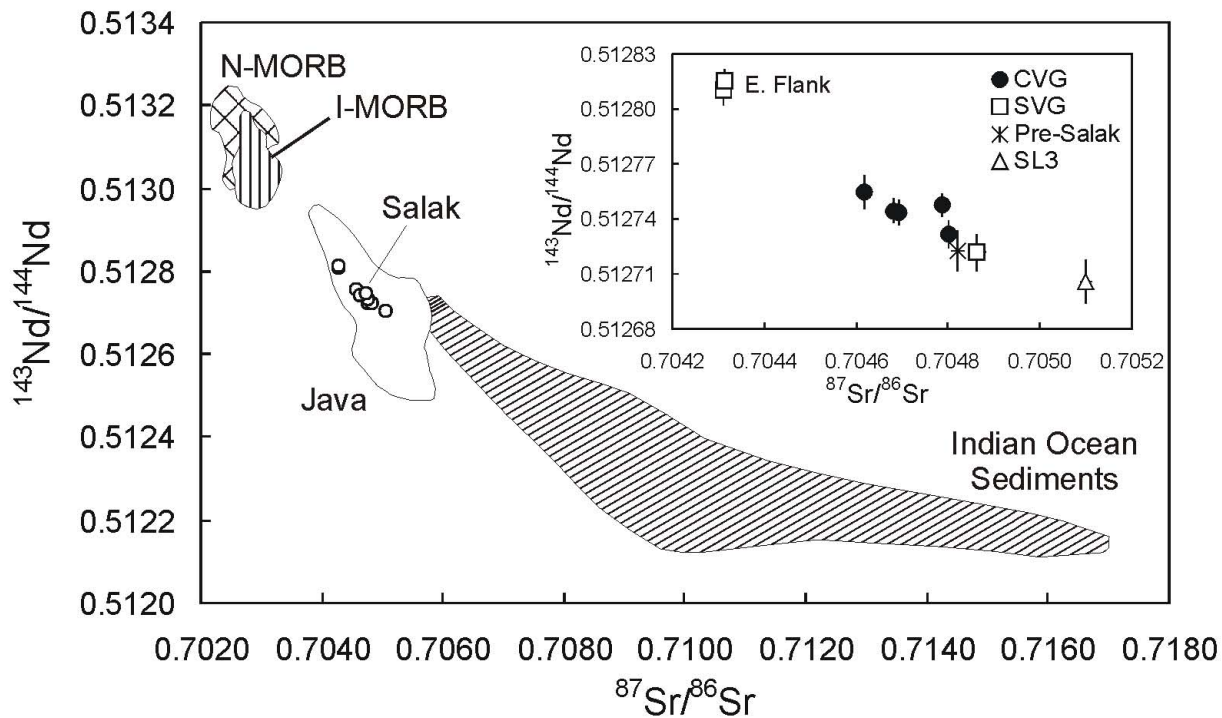


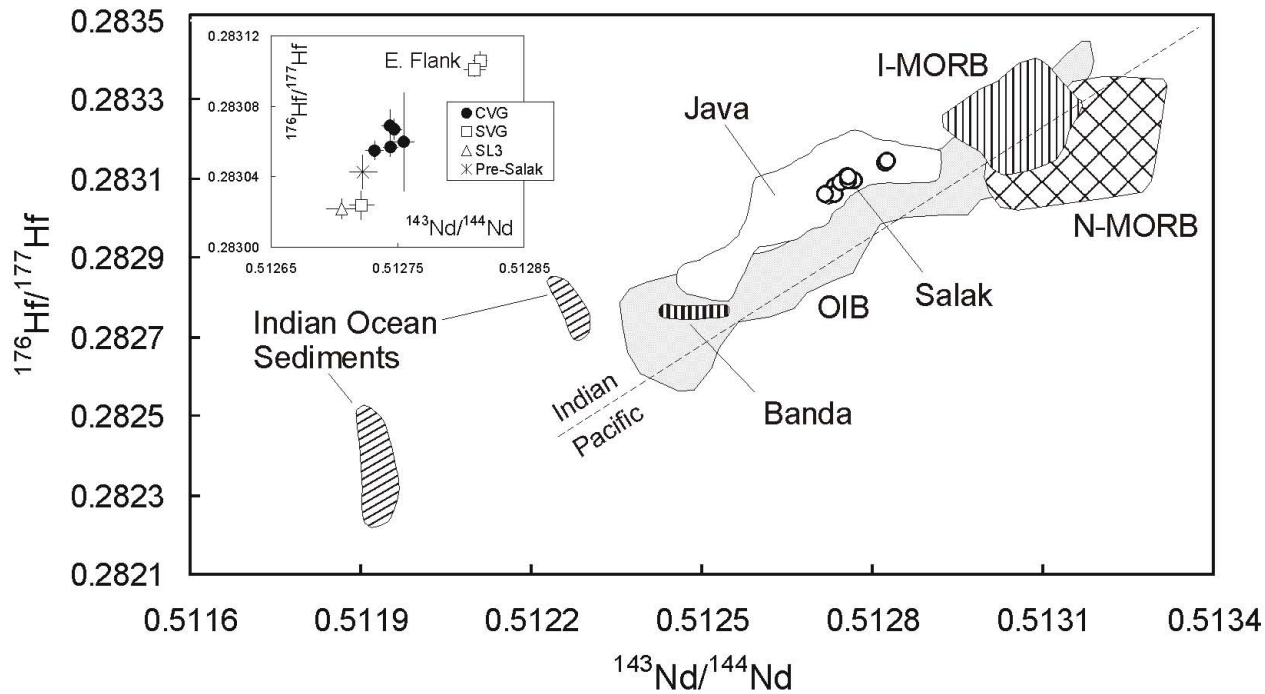


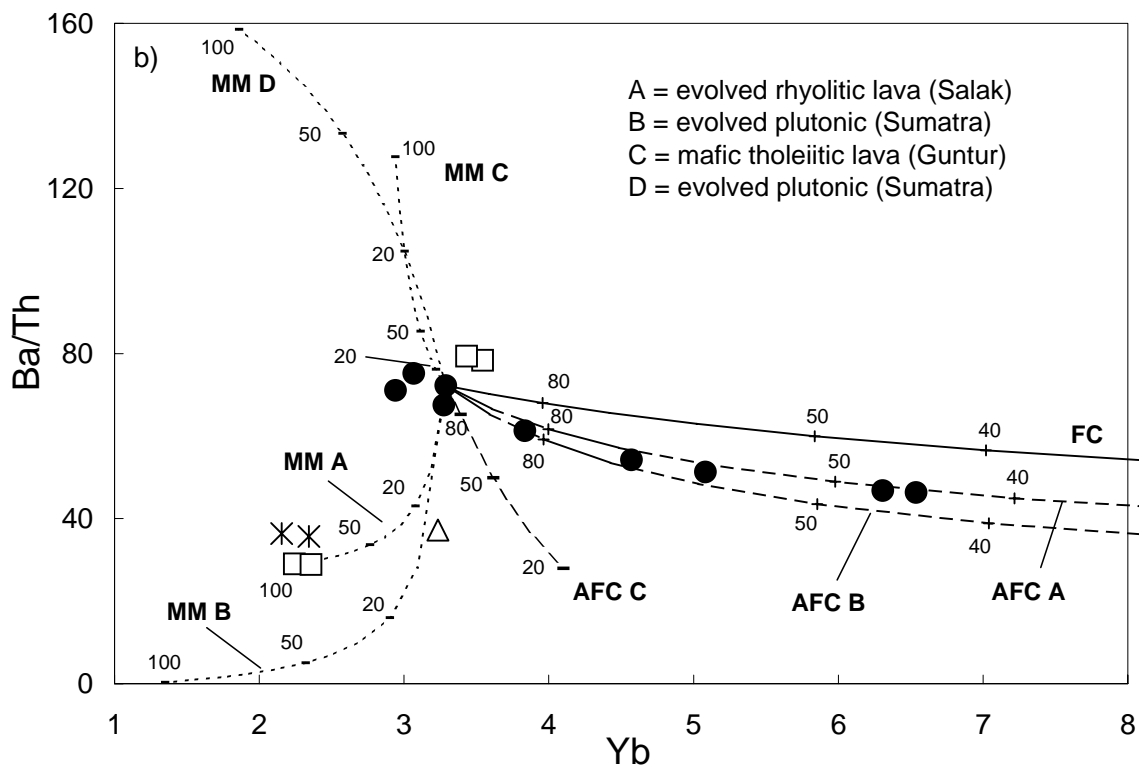
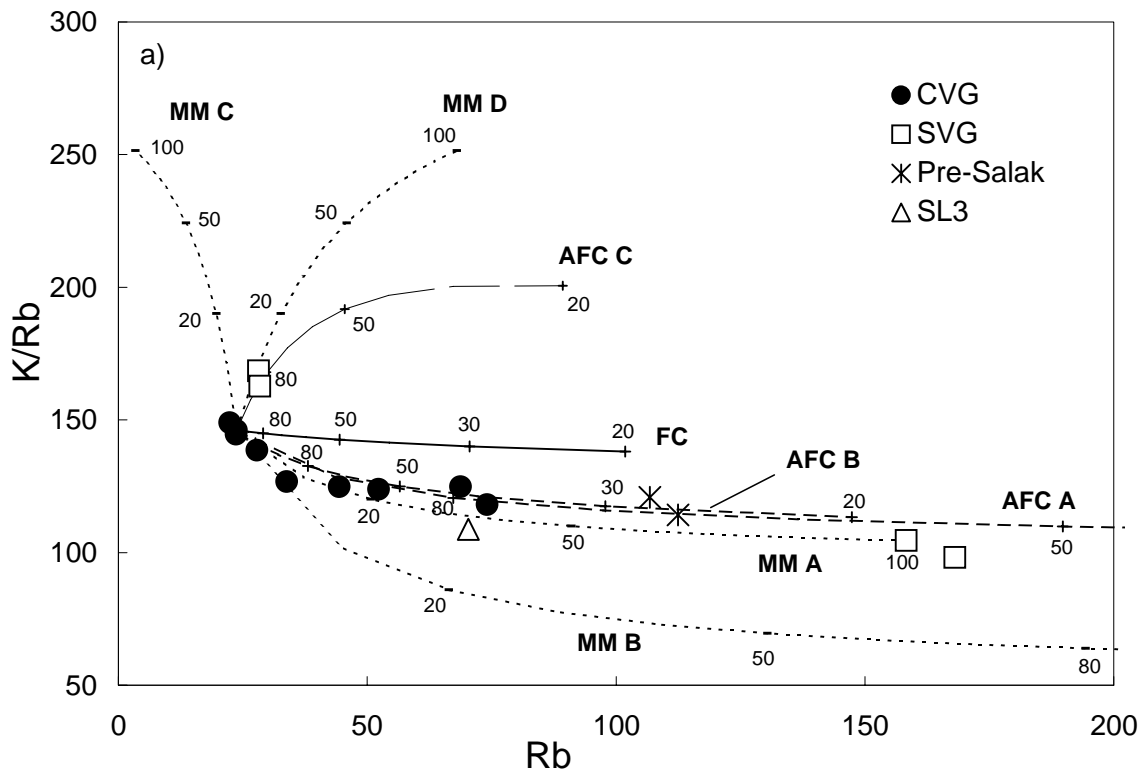


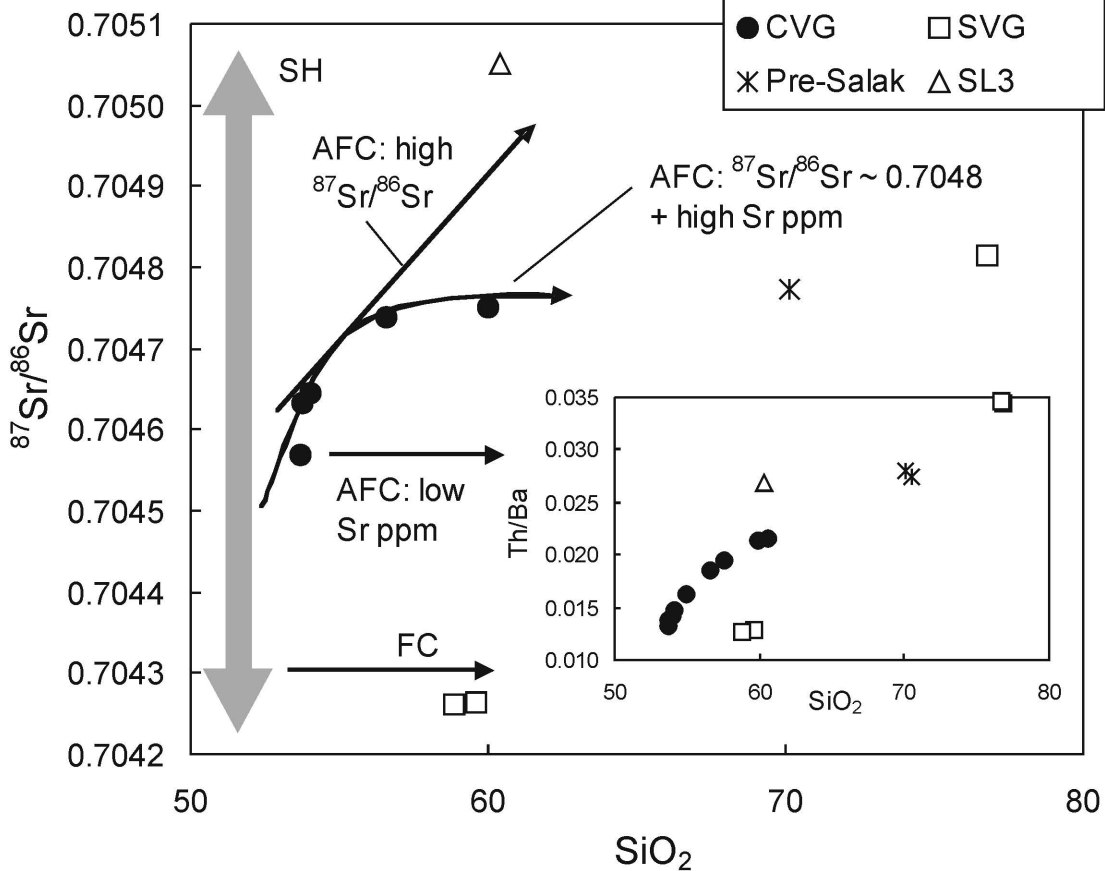


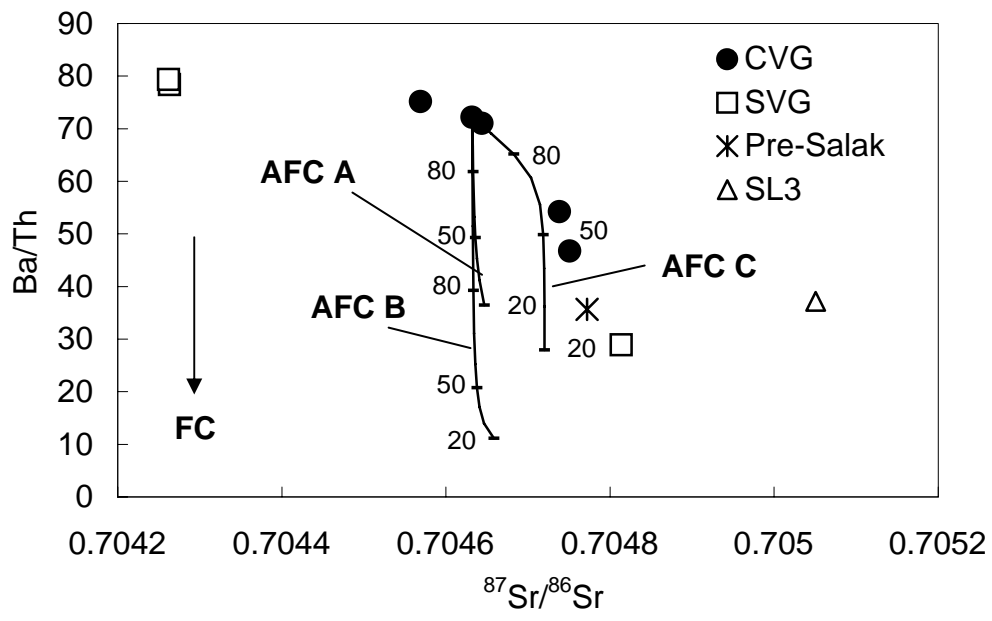












WEST

CVG

EAST

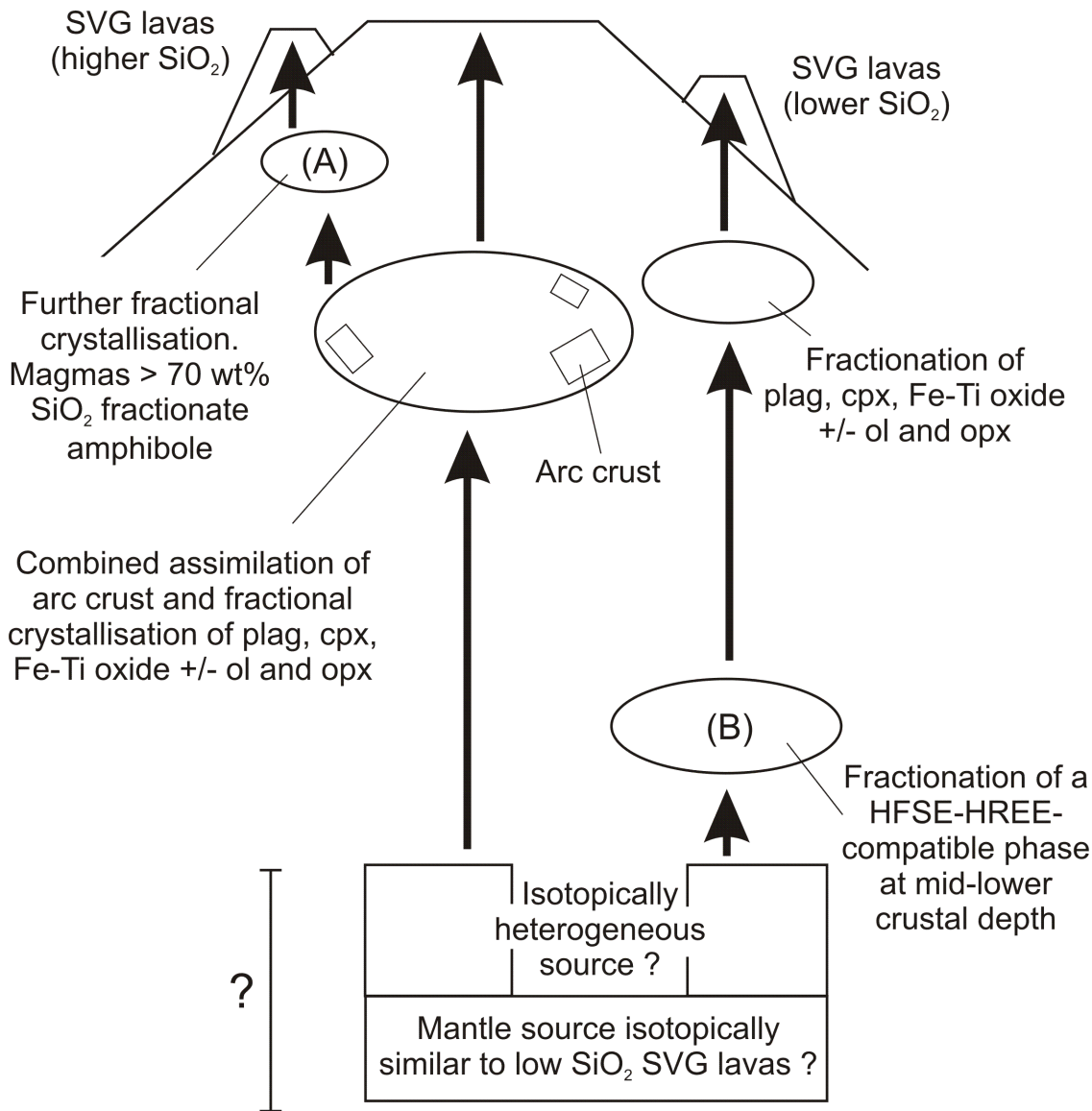


**Table 1**[Click here to download Table: Table\\_1.xls](#)

Table 1

Modal proportions of mineral phases in selected Salak volcanic rocks

	CVG								
	S104	S105	S106A	S106B	S108	S109	S110A	S110B	S111
Ol	2.1	4.2	3.3	3.2	-	1.9	-	-	9.1
Opx	1	0.8	7.2	5.9	2.3	3.2	4.2	3.2	-
Cpx	0.3	0.4	2.1	3.8	1.4	7.1	4.3	2.1	-
Plag	26.4	32.8	31.2	32.3	15.5	28.6	14.3	12.7	31.5
Ox	1.1	1.8	2	2	1.9	2	2.1	1.5	2.1
Hbl	-	-	-	-	-	-	-	-	-
Bio	-	-	-	-	-	-	-	-	-
Qtz	-	-	-	-	-	-	-	-	-
GM	69.1	60	54.2	52.8	78.9	57.2	75.1	80.5	57.3

	SVG				SL3	Pre-Salak
	S102	S103	S107B	S102XEN	S112	S101
Ol	-	-	-	-	-	-
Opx	6.2	10.8	-	2.7	7.4	1.5
Cpx	5.1	9	0.1	4.6	10.2	0.25
Plag	34.3	35.4	4.3	10.3	41.1	8.2
Ox	2.9	3.9	0.5	1.7	4	-
Hbl	-	-	0.25	-	-	0.25
Bio	-	-	0.25	-	-	-
Qtz	-	-	1.5	-	-	0.5
GM	51.5	40.9	93.1	80.7	37.3	89.3

Modal phase volume (%) established from point-counting between 200-300 points per sample. Ol, olivine; Opx, orthopyroxene; Cpx, clinopyroxene; Plag, plagioclase; Ox, Fe-Ti oxide; Hbl, hornblende; Bio, biotite; Qtz, quartz; GM, groundmass; XEN, xenolith.

**Table 2**[Click here to download Table: Table\\_2new.xls](#)

Table 2

## Representative chemical analyses of olivines

Group Sample Grain-Position	CVG			
	S106B INC	S106B P2-M	S111 P2	S111 P3
SiO <sub>2</sub>	36.27	35.09	35.14	36.42
TiO <sub>2</sub>	0.01	0.02	0.05	0.04
Cr <sub>2</sub> O <sub>3</sub>	0.00	0.00	0.00	0.01
MgO	32.79	27.32	25.64	29.66
CaO	0.17	0.19	0.22	0.18
MnO	0.58	0.82	0.82	0.71
FeO	29.60	36.65	38.66	33.94
NiO	0.01	0.01	0.04	0.03
Na <sub>2</sub> O	0.01	0.01	0.00	0.00
Total	99.44	100.10	100.56	100.99
Si	0.99	0.99	0.99	1.00
Fe(ii)	0.67	0.86	0.91	0.78
Mn	0.01	0.02	0.02	0.02
Mg	1.33	1.14	1.08	1.21
Ca	0.00	0.01	0.01	0.01
Total	3.02	3.02	3.01	3.01
Fo	66.39	57.06	54.18	60.91
Fa	33.61	42.94	45.82	39.09

Grain: P#, phenocryst; INC, inclusion.

Position: M, mid point.

Fo, forsterite content; Fa, fayalite content.

Structural formula based on 4 oxygens.

Table 3

[Click here to download Table: Table\\_3new.xls](#)

Table 3

Representative mineral chemical analyses of pyroxenes

Clinopyroxene						Orthopyroxene					
Group	CVG		SVG		SL3	CVG		SVG		SL3	
Sample	S106B	S110B	S102	S102(XEN)	S112	S106B	S110B	S102	S102(XEN)	S102(XEN)	S112
Grain-Position	P1-R	P1	P1*R	P2	P1-M	P1-R	P1	P1-C	P1	P3	P2-C
SiO <sub>2</sub>	49.92	50.64	51.24	52.78	50.99	52.71	51.93	51.68	51.88	53.37	52.25
TiO <sub>2</sub>	0.68	0.70	0.37	0.49	0.26	0.32	0.40	0.21	0.19	0.22	0.23
Al <sub>2</sub> O <sub>3</sub>	3.42	2.21	1.47	1.83	1.07	2.09	1.20	1.00	1.23	0.65	0.88
Cr <sub>2</sub> O <sub>3</sub>	0.00	0.00	0.01	0.00	0.00	0.00	0.01	0.00	0.02	0.02	0.01
Fe <sub>2</sub> O <sub>3</sub>	4.23	3.65	3.70	0.79	3.97	1.73	1.81	2.67	2.18	1.37	2.26
FeO	6.79	9.05	7.36	9.63	7.85	16.50	20.13	21.43	20.81	17.88	20.91
MnO	0.35	0.47	0.50	0.48	0.51	0.48	0.68	1.02	0.92	0.63	0.70
MgO	15.10	14.33	15.54	15.15	13.70	24.80	21.97	21.00	21.54	24.24	21.76
CaO	19.28	19.26	19.48	19.64	21.13	1.63	1.83	1.46	1.49	1.69	1.67
Na <sub>2</sub> O	0.33	0.31	0.23	0.27	0.29	0.01	0.03	0.04	0.03	0.03	0.03
K <sub>2</sub> O	0.00	0.00	0.00	0.01	0.00	0.00	0.00	0.01	0.00	0.00	0.00
NiO	0.01	0.01	0.01	0.00	0.01	0.00	0.00	0.01	0.00	0.00	0.00
Total	100.11	100.61	99.91	101.07	99.78	100.27	99.99	100.52	100.30	100.09	100.70
Si	1.88	1.91	1.93	1.95	1.94	1.93	1.95	1.95	1.95	1.97	1.95
Al	0.15	0.10	0.07	0.08	0.05	0.09	0.05	0.04	0.05	0.03	0.04
Fe(ii)	0.21	0.28	0.23	0.30	0.25	0.50	0.63	0.67	0.65	0.55	0.65
Fe(iii)	0.12	0.10	0.10	0.02	0.11	0.05	0.05	0.08	0.06	0.04	0.06
Cr	0.00	0.00	0.00	0.00	0.00	0.00	0.00	0.00	0.00	0.00	0.00
Ti	0.02	0.02	0.01	0.01	0.01	0.01	0.01	0.01	0.01	0.01	0.01
Mn	0.01	0.02	0.02	0.02	0.02	0.01	0.02	0.03	0.03	0.02	0.02
Mg	0.85	0.80	0.87	0.83	0.78	1.35	1.23	1.18	1.21	1.33	1.21
Ca	0.78	0.78	0.79	0.78	0.86	0.06	0.07	0.06	0.06	0.07	0.07
Na	0.02	0.02	0.02	0.02	0.02	0.00	0.00	0.00	0.00	0.00	0.00
Total	4.04	4.03	4.03	4.01	4.03	4.01	4.01	4.02	4.02	4.01	4.02
Wo	39.54	39.21	39.15	39.94	42.75	3.22	3.68	2.92	2.99	3.33	3.31
En	43.10	40.59	43.45	42.89	38.58	68.25	61.33	58.48	60.10	66.41	60.18
Fs	17.36	20.20	17.40	17.17	18.67	28.53	35.00	38.60	36.91	30.26	36.51

Grain: P#, phenocryst; \*mantling orthopyroxene. XEN = xenolith. Position: C, core; M, mid point; R, rim.

Wo, wollastonite content; En, enstatite content; Fs, ferrosilite content. Structural formula based on 6 oxygens.

Fe(iii) = 2X(1-T/S), where X = number of oxygens, T and S = correct and observed cation totals, respectively.

Table 4

[Click here to download Table: Table\\_4new.xls](#)

Table 4

## Representative mineral chemical analyses of plagioclase

Group	CVG					SVG				SL3	
Sample	S106B	S106B	S110B	S111	S111	S102	S102	S102(XEN)	S102(XEN)	S112	S112
Grain-Position	P3-M	P4-R	P3-C	GM	P4-R	P2-C	P2-R	P2-C	P2-M	P3-C	P3-R
SiO <sub>2</sub>	45.33	51.16	53.97	55.44	45.66	54.69	53.72	53.87	48.00	54.10	52.46
TiO <sub>2</sub>	0.01	0.04	0.05	0.07	0.01	0.04	0.02	0.02	0.03	0.02	0.03
Al <sub>2</sub> O <sub>3</sub>	33.88	29.59	28.19	27.05	34.05	27.57	27.77	28.05	31.69	27.71	28.94
MgO	0.05	0.08	0.07	0.06	0.02	0.05	0.05	0.04	0.07	0.05	0.05
CaO	18.56	13.85	11.90	11.04	18.60	11.09	11.45	11.83	16.37	11.45	13.03
MnO	0.02	0.00	0.02	0.00	0.00	0.01	0.00	0.00	0.00	0.00	0.02
FeO	0.60	0.66	0.59	1.22	0.62	0.41	0.57	0.48	0.51	0.45	0.54
Na <sub>2</sub> O	1.16	3.80	4.97	5.50	1.08	5.42	5.26	4.94	2.41	5.27	4.42
K <sub>2</sub> O	0.03	0.11	0.21	0.31	0.02	0.14	0.13	0.11	0.02	0.22	0.17
Total	99.63	99.29	99.96	100.69	100.05	99.41	98.95	99.34	99.09	99.27	99.64
Si	8.43	9.41	9.81	10.01	8.44	9.96	9.85	9.83	8.91	9.88	9.59
Al	7.42	6.42	6.04	5.76	7.42	5.92	6.00	6.03	6.93	5.97	6.24
Fe	0.09	0.10	0.09	0.18	0.10	0.06	0.09	0.07	0.08	0.07	0.08
Ca	3.70	2.73	2.32	2.14	3.68	2.16	2.25	2.31	3.25	2.24	2.55
Na	0.42	1.36	1.75	1.93	0.39	1.91	1.87	1.75	0.87	1.87	1.57
K	0.01	0.03	0.05	0.07	0.00	0.03	0.03	0.03	0.00	0.05	0.04
Mg	0.01	0.02	0.02	0.02	0.00	0.01	0.01	0.01	0.02	0.01	0.01
Total	20.07	20.06	20.07	20.10	20.04	20.05	20.10	20.04	20.06	20.09	20.09
An	89.72	66.38	56.30	51.69	90.45	52.64	54.20	56.59	78.92	53.87	61.39
Ab	10.13	32.98	42.51	46.61	9.46	46.60	45.06	42.77	20.98	44.89	37.68
Or	0.15	0.63	1.19	1.71	0.09	0.76	0.74	0.64	0.10	1.24	0.93

Grain: P#, phenocryst; GM, groundmass. Position: C, core; M, mid point; R, rim. Structural formula based on 32 oxygens. XEN, xenolith within rock. An, anorthite content; Ab, albite content; Or, orthoclase content.

**Table 5**[Click here to download Table: Table\\_5new.xls](#)

Table 5

Representative mineral chemical analyses of Fe-Ti oxides

Group	CVG									SVG				SL3				
	Sample	S106B	S106B	S106B	S110B	S110B	S110B	S111	S111	S111	S102	S102	S102(XEN)	S102(XEN)	S112	S112	S112	S112
Grain-Position	P1-C	P2-C	P3	INC	P1	P2	P1	P2	P3	P1	P2	P1	P2	P1	P2	P3	P4-C	P4-C
SiO <sub>2</sub>	0.08	0.07	0.07	0.08	0.07	0.08	0.07	0.10	0.05	0.10	0.06	0.05	0.11	0.05	0.05	0.03	0.06	0.04
TiO <sub>2</sub>	11.05	11.32	15.56	15.95	18.18	15.03	10.29	12.77	11.18	11.64	12.85	9.68	46.52	13.32	13.78	13.52	13.45	13.46
Al <sub>2</sub> O <sub>3</sub>	4.24	3.66	1.85	3.11	2.46	2.69	4.37	2.74	3.66	2.41	2.09	2.84	0.05	2.53	2.34	2.39	2.44	2.48
Cr <sub>2</sub> O <sub>3</sub>	0.03	0.05	0.07	0.01	0.04	0.03	0.16	0.24	0.14	0.02	0.01	0.06	0.00	0.03	0.02	0.04	0.02	0.03
Fe <sub>2</sub> O <sub>3</sub>	43.72	43.25	37.35	34.37	31.46	37.93	44.32	41.08	43.62	43.53	41.30	47.13	0.00	41.14	41.01	40.57	40.16	40.84
FeO	37.57	38.13	42.54	41.35	45.19	42.08	37.46	39.94	38.31	39.58	40.24	37.59	46.67	41.53	41.56	40.31	40.31	40.79
MnO	0.43	0.44	0.47	0.51	0.58	0.59	0.40	0.42	0.42	0.52	0.62	0.48	1.26	0.51	0.58	0.52	0.49	0.49
MgO	2.67	2.25	1.82	2.61	1.68	1.96	2.19	1.89	2.11	1.33	1.37	1.50	1.63	1.31	1.60	1.94	1.86	1.77
CaO	0.00	0.00	0.03	0.02	0.00	0.03	0.00	0.01	0.00	0.00	0.02	0.00	0.19	0.01	0.00	0.05	0.00	0.00
Total	99.79	99.15	99.75	98.00	99.66	100.42	99.26	99.19	99.48	99.12	98.55	99.32	96.42	100.42	100.93	99.37	98.79	99.90
Si	0.02	0.02	0.02	0.02	0.02	0.02	0.02	0.03	0.01	0.03	0.02	0.01	0.04	0.02	0.01	0.01	0.02	0.01
Ti	2.43	2.52	3.47	3.58	4.05	3.32	2.28	2.86	2.49	2.63	2.92	2.18	10.78	2.96	3.05	3.03	3.03	3.00
Al	1.46	1.28	0.65	1.09	0.86	0.93	1.52	0.96	1.27	0.85	0.74	1.00	0.02	0.88	0.81	0.84	0.86	0.87
Cr	0.01	0.01	0.02	0.00	0.01	0.01	0.04	0.06	0.03	0.00	0.00	0.01	0.00	0.01	0.01	0.01	0.00	0.01
Fe(iii)	9.62	9.63	8.35	7.71	7.00	8.38	9.84	9.20	9.70	9.83	9.38	10.61	0.00	9.16	9.07	9.08	9.04	9.10
Fe(ii)	9.19	9.44	10.56	10.31	11.18	10.33	9.24	9.94	9.46	9.93	10.16	9.40	12.03	10.27	10.21	10.03	10.09	10.11
Mn	0.11	0.11	0.12	0.13	0.14	0.15	0.10	0.11	0.10	0.13	0.16	0.12	0.33	0.13	0.14	0.13	0.12	0.12
Mg	1.16	0.99	0.81	1.16	0.74	0.86	0.96	0.84	0.93	0.59	0.62	0.67	0.75	0.58	0.70	0.86	0.83	0.78
Ca	0.00	0.00	0.01	0.01	0.00	0.01	0.00	0.00	0.00	0.00	0.01	0.00	0.06	0.00	0.00	0.01	0.00	0.00
Total	24.00	24.00	24.00	24.00	24.00	24.00	24.00	24.00	24.00	24.00	24.00	24.00	24.00	24.00	24.00	24.00	24.00	24.00
TiO <sub>2</sub>	11.97	12.21	16.30	17.40	19.17	15.82	11.17	13.61	12.01	12.29	13.62	10.25	49.92	13.88	14.30	14.32	14.32	14.15
Fe <sub>2</sub> O <sub>3</sub>	47.35	46.66	39.14	37.50	33.17	39.90	48.14	43.80	46.85	45.94	43.75	49.93	0.00	42.86	42.56	42.98	42.76	42.95
FeO	40.69	41.13	44.57	45.11	47.65	44.28	40.69	42.58	41.14	41.77	42.63	39.82	50.08	43.26	43.14	42.70	42.92	42.90

Grain: P, phenocryst; GM, groundmass; GLOM, glomerocryst; INC, inclusion (mineral included within is stated in parentheses) XEN = xenolith.

Spot: C, core; M, mid point (number indicates relative position along transect from core to rim); R, rim. Structural formula based on 32 oxygens.

Table 6

[Click here to download Table: Table\\_6.xls](#)

Table 6

Whole rock major element, trace element and isotopic compositions of Salak volcanic rocks

Sample	CVG								
	S104	S105	S106A	S106B	S108	S109	S110A	S110B	S111
SiO <sub>2</sub>	54.90	54.09	54.01	53.77	57.50	56.58	59.97	60.57	53.66
Al <sub>2</sub> O <sub>3</sub>	19.43	20.16	18.71	18.78	17.49	17.60	15.83	15.94	19.61
Fe <sub>2</sub> O <sub>3</sub>	8.89	8.45	9.99	9.85	8.78	9.21	8.50	8.50	9.60
MgO	2.54	2.49	3.63	3.61	2.26	2.88	1.86	1.81	3.33
CaO	7.70	8.79	8.38	8.39	6.20	6.89	5.14	4.98	8.67
Na <sub>2</sub> O	3.60	3.56	3.35	3.48	4.15	3.85	4.26	4.29	3.32
K <sub>2</sub> O	1.03	0.93	0.83	0.84	1.56	1.34	2.07	2.11	0.80
TiO <sub>2</sub>	1.04	0.97	1.02	1.01	1.15	1.18	1.16	1.17	0.98
MnO	0.17	0.17	0.19	0.19	0.21	0.20	0.19	0.16	0.18
P <sub>2</sub> O <sub>5</sub>	0.33	0.26	0.26	0.26	0.40	0.28	0.48	0.48	0.28
LOI	0.48	-0.13	-0.05	0.05	0.16	0.01	0.08	0.15	-0.08
Total	100.12	99.74	100.32	100.22	99.86	100.01	99.54	100.17	100.36
Sc	23	20	23	23	24	27	24	23	20
Ti	6851	6683	6671	6605	7618	7876	7750	7726	5568
V	160	143	178	177	99	161	75	74	164
Cr	2.2	1.1	2.4	4.3	0.4	0.5	0.3	0.9	7.7
Mn	1262	1239	1727	1743	1928	1835	1750	1193	1495
Co	19	18	22	22	14	17	13	10	21
Ni	4.7	1.5	4.3	4.2	0.8	1.1	1.1	0.9	8.1
Cu	52	26	38	36	38	35	54	41	18
Zn	72	58	70	74	87	73	81	76	70
Ga	20	19	19	19	19	19	19	19	19
Rb	33.8	27.8	23.7	23.8	52.3	44.4	68.8	74.1	22.4
Sr	374	451	422	422	354	358	292	291	395
Y	41	35	32	37	55	52	67	69	33
Zr	188	140	125	125	226	189	311	310	133
Nb	8.15	6.04	5.25	5.21	9.99	7.87	13.67	13.76	5.65
Cs	2.27	0.99	0.75	0.95	2.80	2.31	3.83	4.13	0.78
Ba	214	194	173	176	304	253	368	366	188
La	18.1	13.7	12.9	16.2	22.5	19.2	29.3	30.1	14.0
Ce	41.6	31.9	29.2	29.8	52.1	41.7	68.2	65.9	32.4
Pr	6.07	4.68	4.32	5.20	7.56	6.29	9.76	10.09	4.79
Nd	27.6	21.6	20.0	24.2	34.5	28.7	44.2	45.3	22.2
Sm	6.48	5.20	4.84	5.67	8.33	6.95	10.43	10.65	5.28
Eu	1.86	1.54	1.44	1.68	2.06	1.82	2.33	2.35	1.58
Gd	6.79	5.70	5.25	6.19	8.93	7.50	11.03	11.24	5.68
Tb	1.08	0.91	0.83	0.98	1.45	1.24	1.77	1.83	0.90
Dy	6.52	5.50	4.96	5.83	8.69	7.55	10.67	10.99	5.33
Ho	1.36	1.17	1.05	1.22	1.83	1.63	2.25	2.35	1.13
Er	3.77	3.24	2.90	3.36	5.06	4.56	6.27	6.42	3.09
Tm	0.60	0.51	0.46	0.51	0.79	0.71	0.97	1.02	0.48
Yb	3.84	3.28	2.94	3.29	5.08	4.57	6.31	6.54	3.07
Lu	0.64	0.54	0.49	0.55	0.85	0.77	1.07	1.08	0.52
Hf	4.58	3.58	3.23	3.19	5.82	4.87	7.94	7.93	3.41
Ta	0.47	0.34	0.30	0.31	0.60	0.47	0.81	0.87	0.33
Pb (total)	7.0	6.3	4.7	6.8	13.8	9.2	16.1	22.6	5.3
Th	3.49	2.87	2.44	2.43	5.94	4.66	7.88	7.90	2.51
U	0.81	0.64	0.56	0.56	1.32	1.02	1.72	1.74	0.58
<sup>87</sup> Sr/ <sup>86</sup> Sr <sub>m</sub>			0.704671±9	0.704639±9		0.704745±9	0.704778±10		0.704596±10
<sup>143</sup> Nd/ <sup>144</sup> Nd <sub>m</sub>			0.512735±7	0.512738±6		0.512741±6	0.512723±8		0.512746±9
<sup>176</sup> Hf/ <sup>177</sup> Hf <sub>m</sub>			0.283055±9	0.283040±6		0.283050±6	0.283041±6		0.283046±28

Major element contents in wt%; trace elements concentrations in ppm; <sub>m</sub> = measured; isotope ratios ± 2SE (2\*standard internal error).

**Table 7**[Click here to download Table: Table\\_7.xls](#)

Table 7

Oxygen isotope data ( $\delta^{18}\text{O}$ ) of mineral separates from Salak volcanic rocks

	clinopyroxene	plagioclase
S100		6.03
S103	5.18	5.97
S106A	5.37	
S111		5.96
S112	5.44	6.07

**Table 8**[Click here to download Table: Table\\_8.xls](#)

Table 8

End member compositions used in modelling calculations

Sample	Type	Element Concentrations (ppm)				
		K	Rb	Ba	Th	Yb
S106B	Salak basaltic andesite	3470	24	176	2.4	3.29
A 107A	Salak rhyolite	16545	158	582	20.1	2.24
B 75415	Sumatran granitoid	14652	237	12	34.9	1.35
C GU1/T	Javan tholeiite	1374	3.4	97	0.8	2.94
D 75413	Sumatran granitoid	17101	68	937	5.9	1.86

Sumatran granitoid data from Gasparon (1993); Javan tholeiite from Guntur (Edwards, 1990); Salak samples from this study

Table 9

Summary of least squares major element modelling calculations for CVG rocks

Model		1	2	3	4
Parent		S106B	S106B	S106B	S106B
Daughter		S110B	S108	S104	S104
SiO <sub>2</sub> range (%)		53.8-60.6	53.8-57.5	53.8-54.9	53.8-54.9
$\Sigma r^2$		0.13	0.13	0.01	0.01
% of phase removed relative to initial magma	Plag	43.4	32.9	10.6	8.2
	Cpx	6.0	5.7	4.3	4.5
	Ol	-	-	-	2.7
	Opx	7.9	6.1	3.5	-
	Ox	3.9	3.0	1.6	0.8
%C		61	48	20	16

%C = percentage of crystallisation (sum of phases removed)

The mineral phases considered in modelling are limited to those observed as phenocrysts in either the parent or daughter rocks.

Table 10  
Results of trace element Rayleigh Fractionation modelling

Element	Yb	Ti	Y
normalised phase proportions			
Plag	70.97	70.97	70.97
Opx	12.84	12.84	12.84
Cpx	9.80	9.80	9.80
Fe-Ti Ox	6.40	6.40	6.40
Parent concentration (Co)	3.3	6605	37
Degree of fractionation (F)	0.39	0.39	0.39
$D_{\text{Plag}}$	0.052	0.052	0.076
$D_{\text{Opx}}$	0.283	0.423	0.028
$D_{\text{Cpx}}$	0.661	0.350	0.860
$D_{\text{Fe-Ti Ox}}$	0.218	9.500	0.322
D (bulk)	0.170	0.733	0.203
Calculated daughter comp. (Cl)	<b>7.2</b>	<b>8500</b>	<b>79</b>
Measured daughter comp. (Cl)	<b>6.5</b>	<b>7726</b>	<b>69</b>

Daughter (S110B) composition calculated by forward modelling of parent S106B using  $Cl = Co \cdot F^{(D-1)}$ .

Phase proportions and degree of fractionation values used are those suggested by least squares modelling (Table 9, Model 1). Distribution coefficients (D) are average values for basaltic-dacitic systems from the GERM database (<http://earthref.org/GERM/index.html>).

Table 11

Trace element and  $^{87}\text{Sr}/^{86}\text{Sr}$  isotope compositions of potential crustal contaminants

	Sample no.	Rock Type	Sr (ppm)	$^{87}\text{Sr}/^{86}\text{Sr}$	K/Rb	Ba/Th
1	VM33-75	terrig.-bio. sediment	196	0.70925	106	16
2	VM33-79	terrigenous mud	160	0.70802	124	18
3	CS	calcareous-organogenic sediment	1258	~ 0.709	106	60
4	76100	S-Type granite	32	0.74036	185	0.2
5	ME99AL16	intrusive (51 wt % $\text{SiO}_2$ )	609	0.706155	118	77
6	ME00AL42	intrusive (62 wt % $\text{SiO}_2$ )	375	0.706600	126	53
7	H110x	intrusive (51 wt % $\text{SiO}_2$ )	152	0.708561	139	292
8	J82x	intrusive (hbl spessarite)	173	0.705291	346	58
9	GU1/T	Javan tholeiitic lava	232	0.70393	404	127
10	TAF43/6	Tongan tholeiitic lava	118	0.70388	519	344
11	417D-418A	altered oceanic crust	118	0.704584	235	364
12	M22	basalt (ophiolitic)	143	-	416 <sup>a</sup>	10
13	P-15	dolerite (ophiolitic)	171	-	4150	27
14	S-134	clinopyroxene gabbro (ophiolitic)	129	-	1245	70

Data sources: 1-4: Gasparon 1993; Gasparon et al., 1998; 5-8: Elburg et al., 2005; 9: (Guntur tholeiite) Edwards, 1990; 10: Turner et al., 1997; 11: (average 417D-418A n = 7) Staudigel et al., 1996; 12-14 (Sulawesi ophiolite) Kadarusman et al., 2004.

<sup>a</sup> Rb concentration below detection limit therefore Rb abundance used is of sample P-33 (0.5 ppm) from the same area.